

Iterative LMMSE Channel Estimation, Multiuser Detection, and Decoding via Spatial Coupling

Keigo Takeuchi, *Member, IEEE*

Abstract—Spatial coupling is utilized to improve the performance of iterative channel estimation, multiuser detection, and decoding for multiple-input multiple-output (MIMO) bit-interleaved coded modulation (BICM). Coupling is applied to both coding and BICM—the encoder uses a protograph-based spatially-coupled low-density parity-check (SC LDPC) code. Spatially and temporally coupled (STC) BICM is proposed to enable iterative channel estimation via coupling. Linear minimum mean-squared error (LMMSE) estimation is applied for both channel estimation and detection to reduce the complexity. Tractable density evolution (DE) equations are derived to analyze the convergence property of iterative receivers in the large-system limit, via a tool developed in statistical physics—replica method. The DE analysis implies that the STC BICM can improve the performance of iterative channel estimation especially for higher-order modulation. Numerical simulations show that the STC BICM can provide a significant gain of the performance at high signal-to-noise ratios for 64 quadrature amplitude modulation (QAM), as well as an improvement in the decoding threshold, compared to conventional BICM.

Index Terms—Spatial coupling, multiple-input multiple-output (MIMO) systems, iterative channel estimation, replica method, density evolution.

I. INTRODUCTION

HIGH spectral efficiency is required in modern wireless communications. Multiple-input multiple-output (MIMO) transmission [1], [2] has been used to achieve high spectral efficiency. The channel capacity of MIMO systems grows in proportion to the minimum of the numbers of transmit and receive antennas [2]. It is an important issue to construct low-complexity receivers that realize this potential.

Since the invention of turbo codes [3], iterative multiuser detection and decoding (MUDD) [4], [5] has been proposed as a promising scheme for solving that issue. When bit-interleaved coded modulation (BICM) is used, iterative MUDD can be formulated in a unified framework based on belief propagation (BP) [6], [7]. The optimal symbol-wise maximum-a-posteriori (MAP) detection results in high complexity, so that the linear minimum mean-squared error (LMMSE) detection has been used instead in [8]. The iterative LMMSE MUDD can achieve excellent decoding performance in spite of its low complexity.

Iterative MUDD based on BICM has been extended to iterative channel estimation and MUDD (CE-MUDD) [9]–[15].

The work of K. Takeuchi was in part supported by the Grant-in-Aid for Young Scientists (A) (MEXT/JSPS KAKENHI Grant Number 26709029), Japan.

K. Takeuchi is with the Department of Communication Engineering and Informatics, the University of Electro-Communications, Tokyo 182-8585, Japan (e-mail: ktakeuchi@uec.ac.jp).

Since the optimal nonlinear channel estimator has impractical complexity, the LMMSE channel estimator [13], [14] has been used instead, as considered in iterative MUDD. The iterative LMMSE CE-MUDD can provide a significant reduction of the overhead for training.

In this paper, we improve the performance of iterative CE-MUDD for MIMO BICM systems via spatial coupling. Spatial coupling¹ was proposed as a sophisticated technique for improving the BP performance of low-density parity-check (LDPC) codes up to the MAP performance [16], [17]. A spatially coupled (SC) LDPC code is constructed as a chain of multiple LDPC codes. Both ends of the chain are terminated so that the bits at both ends are decoded successfully. The reliable information at both ends can propagate toward the center of the chain without error propagation, when the code length in each section of the chain is sufficiently long. The rate loss due to the termination is negligible when the chain is sufficiently long. As a result, the BP decoder for the SC LDPC code can achieve the MAP performance of the underlying LDPC code. This improvement in performance via spatial coupling is *universal* [18]–[23], and spatial coupling has been applied to many other problems [20], [24]–[31]. As one more application, spatial coupling is used to improve the performance of iterative CE-MUDD for MIMO systems with no channel state information (CSI).

We apply coupling to both coding and BICM—we use a protograph-based SC LDPC code [17] in coding and a coupled interleaver in BICM. SC LDPC coding was applied to iterative MUDD for MIMO systems [32]. On the other hand, coupled interleavers were proposed to improve the performance of iterative MUDD for LDPC-coded MIMO systems with perfect CSI at the receiver [33] and of iterative channel estimation and decoding for single-antenna systems [34]. In this paper, we propose spatially and temporally coupled (STC) BICM to improve the performance of iterative CE-MUDD.

The purpose of this paper is to investigate whether coupling should be introduced for coding or BICM. In previous works, spatial coupling was applied to either coding or BICM. However, to the best of author’s knowledge, there are no comparisons between the two SC systems. In this paper, we introduce coupling for both coding and BICM, and elucidate whether coupling should be used in coding or BICM.

Density evolution (DE) is used to analyze the performance

¹ Coupling is actually made in the temporal domain for coding. Thus, spatial coupling for coding should be regarded as technical terminology. On the other hand, coupling we introduce for BICM is in the spatial domain for MUDD, whereas it is in the temporal domain for channel estimation.

of iterative CE-MUDD for MIMO systems with SC LDPC coding and STC BICM. DE is a powerful method for analyzing the convergence property of the BP decoder for LDPC codes or turbo codes when the code length tends to infinity [35]–[38]. The method has been used to analyze iterative MUDD [7], [39], iterative channel estimation [40], [41] for single-input single-output systems, and iterative CE-MUDD [42] for code-division multiple-access (CDMA) systems. We extend the DE analysis to the case of iterative CE-MUDD for MIMO systems with SC LDPC coding and STC BICM.

The DE analysis for iterative MUDD cannot yield *analytical* DE equations for describing the convergence property as long as the system size is finite. Consequently, Monte Carlo simulations are required for solving the DE equations. In order to circumvent this difficulty, the large-system limit has been considered [39], [42], in which the numbers of transmit and receive antennas tend to infinity at the same rate. The large-system analysis results in analytical DE equations, which can provide a good approximation for small MIMO systems [43].

In this paper, the replica method is used for the large-system analysis. The method was originally developed in statistical physics [44], [45], and introduced in the field of communications by Tanaka [46]. Then, the replica method has been used for the large-system analysis of MIMO systems with perfect CSI [47]–[51]. MIMO systems with no CSI have been analyzed in [43], [52]. In this paper, the large-system analysis in [43] is applied to the case of MIMO systems with STC BICM. We note that the replica method is based on several non-rigorous assumptions, although it is believed in the literature that the replica method provides correct results.

The contribution of this paper is to present an answer to the main question—whether coupling should be introduced for coding or BICM? We will show that STC BICM hardly improves the performance of iterative CE-MUDD for quadrature phase shift keying (QPSK), when SC LDPC coding is used. This result means that, for QPSK, it is sufficient to introduce coupling only in coding. For higher-order modulation, STC BICM can improve the performance of iterative CE-MUDD even when SC LDPC coding is used. Thus, we claim that coupling should be introduced for BICM or for both coding and BICM if MIMO systems with higher-order modulation are used.

The remainder of this paper is organized as follows: After summarizing the notation used in this paper, In Section II we present MIMO systems with SC LDPC coding and STC BICM. In Section III we derive an iterative LMMSE CE-MUDD algorithm based on approximate BP. In Section IV the DE analysis of the iterative CE-MUDD is performed with the replica method. After presenting comparisons between conventional BICM and STC BICM in Section V, we conclude this paper in Section VI.

Throughout this paper, \mathbf{A}^T and \mathbf{A}^H denote the transpose and conjugate transpose of a matrix \mathbf{A} , respectively. The complex conjugate of a complex number z is denoted by z^* . We write a proper complex Gaussian distribution with mean \mathbf{m} and covariance $\mathbf{\Sigma}$ as $\mathcal{CN}(\mathbf{m}, \mathbf{\Sigma})$. For integers i and j ($i < j$), $[i : j]$ represents the set of integers $\{i, i + 1, \dots, j - 1\}$. The set $[i : j] = \{i, \dots, j\}$ is defined in the same manner. The

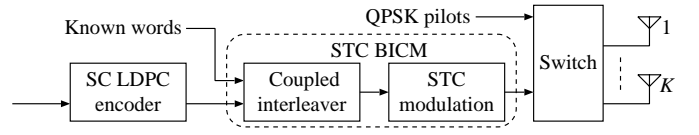


Fig. 1. SC-LDPC-coded MIMO STC BICM.

notation $f(x) \propto g(x)$ implies that there is a positive constant $A > 0$ such that $f(x) = Ag(x)$ for any x .

II. SYSTEM MODEL

A. MIMO System

We consider point-to-point MIMO systems with K transmit antennas and N receive antennas. For simplicity, block-fading channels with coherence time T are assumed—the channel matrix is fixed during T symbol periods, and changes independently at the beginning of the next fading block. This channel model may be regarded as a mathematical model for time-division multiple-access (TDMA) or frequency-hopping systems [53]. Furthermore, we assume independent Rayleigh fading. The channel matrix $\mathbf{H}(b) \in \mathbb{C}^{N \times K}$ in each fading block b has independent circularly symmetric complex Gaussian (CSCG) random elements with variance $1/K$. We note that the latter assumption is an idealized assumption to simplify the large-system analysis. There may be dependencies between the elements in practice. Under these assumptions, the received vector $\mathbf{y}_t(b) \in \mathbb{C}^N$ in symbol period $t \in [1 : T]$ within fading block b is given by

$$\mathbf{y}_t(b) = \mathbf{H}(b)\mathbf{x}_t(b) + \mathbf{w}_t(b). \quad (1)$$

In (1), $\mathbf{x}_t(b) = (x_{1,t}(b), \dots, x_{K,t}(b))^T$ denotes the transmitted vector in symbol period t within fading block b . Furthermore, $\mathbf{w}_t(b) \sim \mathcal{CN}(\mathbf{0}, N_0\mathbf{I}_N)$ is independent additive white Gaussian noise (AWGN) vectors with covariance $N_0\mathbf{I}_N$ in the same symbol period. The channel matrices are unknown to the receiver in advance, whereas all statistical properties are assumed to be known.

The MIMO channel (1) can be expressed in matrix form as

$$\mathbf{Y}(b) = \mathbf{H}(b)\mathbf{X}(b) + \mathbf{W}(b), \quad (2)$$

with the received matrix $\mathbf{Y}(b) = (\mathbf{y}_1(b), \dots, \mathbf{y}_T(b))$, the transmitted matrix $\mathbf{X}(b) = (\mathbf{x}_1(b), \dots, \mathbf{x}_T(b))$, and the AWGN matrix $\mathbf{W}(b) = (\mathbf{w}_1(b), \dots, \mathbf{w}_T(b))$.

We consider a pilot-assisted MIMO STC BICM scheme, shown in Fig. 1. In order to estimate the channel matrices, the first T_{tr} symbol periods in each fading block are assigned to transmission of QPSK pilot symbols with unit power $|x_{k,t}(b)|^2 = 1$, so that the matrix $\mathbf{X}_{[1:T_{\text{tr}}]}(b) = (\mathbf{x}_1(b), \dots, \mathbf{x}_{T_{\text{tr}}}(b))$ in the training period $t \in [1 : T_{\text{tr}}]$ is assumed to be known for all b . The remaining symbol periods are assigned to transmission of data symbols. In the following sections, we present the details of the SC LDPC encoder and the STC BICM.

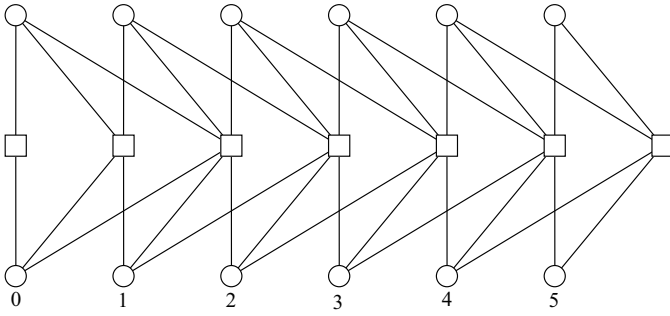


Fig. 2. Protograph for $(3, 6, 6)$ ensemble of SC LDPC codes. The variable and check nodes are represented by circles and boxes, respectively.

B. Spatially Coupled LDPC Codes

We shall review the ensemble of protograph-based SC LDPC codes with the degree of variable nodes d_v , the degree of check nodes d_c , and the number of sections L . Efficient termination [54] is used to reduce the computational complexity in encoding. We refer to this ensemble as (d_v, d_c, L) ensemble. See Fig. 2 for an example of the protograph that represents the $(3, 6, 6)$ ensemble, which is defined via the $(L+1) \times (d_c/d_v)L$ base matrix

$$B = \begin{pmatrix} 1 & 1 & 0 & 0 & 0 & 0 & 0 & 0 & 0 & 0 & 0 & 0 & 0 \\ 1 & 1 & 1 & 1 & 0 & 0 & 0 & 0 & 0 & 0 & 0 & 0 & 0 \\ 1 & 1 & 1 & 1 & 1 & 1 & 0 & 0 & 0 & 0 & 0 & 0 & 0 \\ 0 & 0 & 1 & 1 & 1 & 1 & 1 & 1 & 0 & 0 & 0 & 0 & 0 \\ 0 & 0 & 0 & 0 & 1 & 1 & 1 & 1 & 1 & 1 & 0 & 0 & 0 \\ 0 & 0 & 0 & 0 & 0 & 0 & 1 & 1 & 1 & 1 & 1 & 1 & 1 \\ 0 & 0 & 0 & 0 & 0 & 0 & 0 & 0 & 1 & 1 & 1 & 1 & 1 \end{pmatrix}. \quad (3)$$

The base matrix is obtained by removing the last $(d_v - 2)$ rows of the conventional $(L + d_v - 1) \times (d_c/d_v)L$ base matrix proposed in [17]. Removing the last rows results in performance degradation for finite-length codes, whereas the decoding threshold does not change [54]. Roughly speaking, only reliable information at the left end propagates to the right side of the protograph when the signal-to-noise ratio (SNR) is close to the decoding threshold. The only reason why we use this ensemble is to reduce the encoding complexity in numerical simulations. It is straightforward to replace our results by those for the conventional ensemble without efficient termination [17] if another efficient method for encoding is available in the future.

A parity-check matrix is generated from the base matrix (3) as follows: We replace all ones in the base matrix with $(d_v/d_c)M \times (d_v/d_c)M$ random permutation matrices independently. On the other hand, all zeros are replaced by all-zero matrices with the same size. The obtained $(L+1)(d_v/d_c)M \times LM$ parity-check matrix corresponds to an SC factor graph with L sections. The design rate r of the obtained SC LDPC code is given by

$$r = 1 - \frac{d_v}{d_c} - \frac{d_v}{d_c L}, \quad (4)$$

which tends to the design rate $1 - d_v/d_c$ of the underlying LDPC code as $L \rightarrow \infty$.

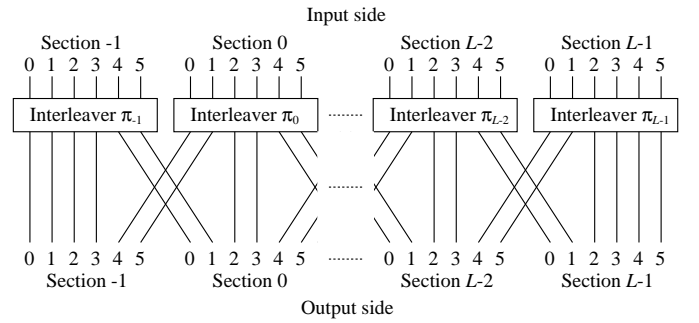


Fig. 3. Coupled interleaver for $M = 6$ and $W = 1$.

In section $l \in \{0, \dots, L-1\}$ the graph has M variable nodes, which are called a codeword in the section. Thus, the overall codeword of an SC LDPC code consists of L codewords.

C. Spatially and Temporally Coupled BICM

1) *Coupled Interleaver*: As the first part of the STC BICM, we define coupled interleavers, which is slightly different from those proposed in [33], [34]. Before presenting coupled interleavers, we shall introduce the ensemble of random interleavers. An interleaver of length M is a permutation of $\mathcal{M} = \{0, 1, \dots, M-1\}$. The ensemble of random interleavers consists of all possible permutations of \mathcal{M} . Each interleaver is picked up from the ensemble uniformly and randomly. It is known that performance for individual interleavers converges almost surely to its average over the ensemble when the length M tends to infinity [7], [39]. Thus, it is sufficient to investigate the average performance over the ensemble, instead of performance for individual interleavers.

Let $L+W$ and W denote the number of sections and coupling width, respectively. A coupled interleaver is constructed as follows: We first generate $L+W$ independent interleavers of length M , and refer to the l th interleaver as section l at the input side for $l \in \mathcal{L} = \{-W, -W+1, \dots, L-1\}$. Each section is divided into $2W+1$ subsections with size $\tilde{M} = M/(2W+1)$. Bit $\mu \in \tilde{\mathcal{M}} = \{0, \dots, \tilde{M}-1\}$ in subsection $w \in \mathcal{W} = \{-W, -W+1, \dots, W\}$ corresponds to the bit $m = \mu + (w+W)\tilde{M} \in \mathcal{M}$ in the same section. Equivalently, bit $m \in \mathcal{M}$ in each section corresponds to the bit $\mu(m) = m - (w(m)+W)\tilde{M}$ in the subsection $w(m) = \lfloor m/\tilde{M} \rfloor - W \in \mathcal{W}$. Subsection $w \in \mathcal{W}$ in section $l \in \mathcal{L}$ is *coupled* with subsection $-w$ in section $l+w$ at the output side for $w \in \mathcal{W}$. If $l+w \notin \mathcal{L}$, it is coupled with subsection w in section l . The (M, L, W) interleaver is formally defined as follows:

Definition 1 ((M, L, W) Interleaver). *A coupled interleaver π is a bijection from $\mathcal{M} \times \mathcal{L}$ onto $\tilde{\mathcal{M}} \times \mathcal{L} \times \mathcal{W}$. Picked up $L+W$ interleavers $\{\pi_l : l \in \mathcal{L}\}$ of length M from the ensemble of random interleavers uniformly and randomly. Let $\mu(\tilde{m}) \in \tilde{\mathcal{M}}$ and $w(\tilde{m}) \in \mathcal{W}$ denote the bit and subsection that correspond to the output bit $\tilde{m} = \pi_l(m) \in \mathcal{M}$. For $(m, l) \in \mathcal{M} \times \mathcal{L}$, the*

coupled interleaver $\pi(m, l)$ is given by

$$\pi(m, l) = \begin{cases} (\mu(\tilde{m}), l + w(\tilde{m}), -w(\tilde{m})) & \text{for } l + w(\tilde{m}) \in \mathcal{L} \\ (\mu(\tilde{m}), l, w(\tilde{m})) & \text{for } l + w(\tilde{m}) \notin \mathcal{L}, \end{cases} \quad (5)$$

with $\tilde{m} = \pi_l(m) \in \mathcal{M}$.

See Fig. 3 for the $(6, L, 1)$ interleaver. We note that the (M, L, W) -interleaver reduces to conventional random interleavers for $W = 0$.

Known words are sent in sections l for $l < 0$ in order to start up iterative CE-MUDD via coupling. On the other hand, the codeword in section l of the SC LDPC code is transmitted in section l of the coupled interleaver for the remaining sections $l \in \{0, \dots, L-1\}$. Note that no known words are transmitted in the opposite end, because of the termination structure (3) of SC LDPC codes.

2) *Spatially and Temporally Coupled Modulation*: We next present the mapping method from the interleaved bit sequences to data matrices. Each data matrix is generated so as to satisfy two conditions. One condition is that each data symbol originates from a codeword in the same section. The other condition is that data symbols generated from different codewords are included in each $K \times (T - T_{\text{tr}})$ data matrix with spatially and temporally uniform probability. The terminology ‘‘STC’’ BICM² originates from the latter condition. The former condition simplifies the DE analysis. See [55] for a relaxation of the former condition.

We consider a constellation $\mathcal{C} \subset \mathbb{C}$ with modulation degree $Q = \log_2 |\mathcal{C}| \in \mathbb{N}$. Our approach for satisfying the two conditions is as follows: Q bits in each subsection are mapped to one data symbol in order to satisfy the former condition. If a data symbol originates from the bits in subsection $w \in W$ (respectively (resp. W)), the next symbol is generated from the bits in the next subsection $w+1$ (resp. $-W$). Assume that the number K of transmit antennas is a multiple of the number $2W+1$ of subsections, or that K tends to infinity with W fixed. When the data symbols are transmitted with K transmit antennas after the generation of every K data symbols, the data symbols in the same symbol period originate from different codewords with equal frequency.

In order to realize uniformity in the temporal domain, we propose an assignment with a cyclic shift. In the proposed assignment, the first K data symbols are transmitted from the transmit antennas k in the order $k = 1, \dots, K$. The next K symbols are assigned to the transmit antennas k in the order $k = 2, \dots, K, 1$, which is a cyclic shift of the assignment in the preceding symbol period. Such assignments with the cyclic shift are repeated for all symbol periods. Assume that K and $T - T_{\text{tr}}$ are a multiple of $2W+1$, or that K and $T - T_{\text{tr}}$ tend to infinity at the same rate. Then, each data stream contains data symbols originating from different codewords with equal frequency.

If assignments with no cyclic shift were used, each transmit antenna would continue to emit the data symbols originating from the same codeword when K is a multiple of $2W+1$. This implies that the channel estimator cannot utilize *reliable*

decisions of the symbols in data streams—originating from the neighboring sections—to estimate the channel gains for the other data streams. Consequently, coupling could not work for channel estimation. We use the assignment with the cyclic shift to avoid such a defect.

We refer to the ensemble of all possible STC BICM schemes—induced by the randomness of coupled interleavers (5)—as the (M, L, W, Q) STC BICM ensemble.

D. Summary of Transmitter

The data matrices are generated via (d_v, d_c, L) SC LDPC coding and (M, L, W, Q) STC BICM. Known binary words $\mathcal{U}_{[-W:0]} = \{\mathbf{u}_l \in \mathbb{F}_2^M : l \in [-W : 0]\}$ of length M are used for the first W sections of the coupled interleaver. For the remaining sections, L codewords $\mathcal{U}_{[0:L]} = \{\mathbf{u}_l \in \mathbb{F}_2^M : l \in [0 : L]\}$ of length M are generated with the SC LDPC code. Then, these $L+W$ binary sequences are interleaved with the coupled interleaver. The interleaved bit sequence in each section is mapped to M/Q data symbols with unit average power, as presented in Section II-C. In this paper, we only consider 2^Q quadrature amplitude modulation (QAM) with Gray mapping for an even number Q . In order to minimize the decoding latency, the codewords are transmitted in the same order as that in decoding. The overall transmission rate is given by

$$R = \left(1 - \frac{T_{\text{tr}}}{T}\right) \left(1 - \frac{W}{L+W}\right) QKr, \quad (6)$$

where r denotes the design coding rate, given by (4) for (d_v, d_c, L) SC LDPC codes.

III. ITERATIVE RECEIVERS

A. Iterative CE-MUDD

The goal of the receiver is to estimate all codewords $\mathcal{U}_{[0:L]}$ from all received matrices $\mathcal{Y} = \{\mathbf{Y}(b) : \text{all } b\}$, all pilot matrices $\mathcal{X}_{[1:T_{\text{tr}}]} = \{\mathbf{X}_{[1:T_{\text{tr}}]}(b) : \text{all } b\}$, and all known words $\mathcal{U}_{[-W:0]}$. We shall derive low-complexity iterative receivers based on approximate BP. The iterative receivers consist of the soft mapper, the LMMSE channel estimator, the LMMSE demodulator, the soft demapper, and the BP decoder, as shown in Fig. 4. The channel estimator calculates approximate a posteriori probability density functions (pdfs) of the channel matrices, and sends them to the demodulator. The demodulator uses the a posteriori pdfs and the received matrices to calculate approximate a posteriori distributions for the data symbols. The a posteriori distributions are fed forward to the soft demapper to calculate the log likelihood ratio (LLR) for each bit of the codewords. The LLRs are used as the a priori LLRs in the BP decoder to calculate extrinsic LLRs. The extrinsic LLRs are fed back to the soft mapper and demapper in order to refine the initial estimates. After several iterations, the BP decoder decodes the codewords on the basis of the a posteriori LLRs. In this paper, we refer to iterations in the BP decoder and in the CE-MUDD as inner and outer iterations, respectively.

We hereafter focus on detection of the k th data symbol $x_{k,t}(b)$ in symbol period t within a fading block b . For notational convenience, we omit the index b .

² One should not confuse STC BICM with space-time coded BICM.

is equivalent to feeding the LMMSE estimate (16) and the a posteriori covariance (17) forward to the demodulator.

Remark 1. Using a mismatched value $\tilde{N}_0 \neq N_0$ should result in no improvement in the decoding threshold, since the LMMSE channel estimator with $\tilde{N}_0 = N_0$ can achieve the non-linear minimum mean-squared error (MMSE) performance in the large-system limit [43]. Thus, we assume $\tilde{N}_0 = N_0$ in the large-system analysis after taking the limit $M \rightarrow \infty$. In order to avoid error propagation for finite-sized systems, on the other hand, we may use a mismatched value $\tilde{N}_0 \neq N_0$ in numerical simulations. By definition, the covariance matrix (14) vanishes as the a priori variances $\{\sigma_{k,t}^2\}$ of the data symbols tend to zero. This typically occurs in the high SNR regime, in which the inverse matrix $(\mathbf{\Xi}_{\setminus t}^{\text{ch}} + \tilde{N}_0 \mathbf{I}_{T-1})^{-1}$ in (16) and (17) diverges when $\tilde{N}_0 = N_0$ is assumed. This divergence may result in error propagation for finite-sized systems. In order to circumvent the divergence, we may use a fixed value $\tilde{N}_0 > 0$ in the high SNR regime, whereas we set $\tilde{N}_0 = N_0$ in the other SNR regime. Note that a mismatched value \tilde{N}_0 is used only for the channel estimator. We always assume $\tilde{N}_0 = N_0$ in the demodulator, since such a divergence does not occur for the demodulator as long as the channel estimator uses a mismatched value $\tilde{N}_0 \neq N_0$.

D. LMMSE Demodulator

We are focusing on the k th data symbol $x_{k,t}$ in symbol period t . Suppose that the soft decisions $\{\hat{x}_{k',t}\}$ and the a priori variances $\{\sigma_{k',t}^2\}$ have been provided by the soft mapper, and that the a posteriori pdf $p(\mathbf{H}|\mathbf{Y}_{\setminus t}, \hat{\mathbf{X}}_{\setminus t})$ sent by the channel estimator is used as the a priori pdf of the channel matrix.

In order to obtain a tractable a posteriori distribution of the data symbol $x_{k,t}$, we shall make the same approximation as in the derivation of the LMMSE channel estimator. We first decompose the first term on the RHS of (1) into two terms,

$$\mathbf{y}_t = \hat{\mathbf{H}}_{\setminus t} \mathbf{x}_t + (\mathbf{H} - \hat{\mathbf{H}}_{\setminus t}) \mathbf{x}_t + \mathbf{w}_t, \quad (18)$$

where the LMMSE channel estimate $\hat{\mathbf{H}}_{\setminus t}$ is given by (16). We next approximate the second term by a CSCG term with covariance $\zeta_t \mathbf{I}_N$, given by

$$\zeta_t = \text{Tr} \left(\mathbf{\Xi}_{\setminus t}^{\text{ch}} \text{diag} \{ \sigma_{k',t}^2 + |\hat{x}_{k',t}|^2 : \text{for all } k' \} \right), \quad (19)$$

where $\mathbf{\Xi}_{\setminus t}^{\text{ch}}$ is given by (17). The obtained approximate MIMO channel can be regarded as a MIMO channel with the known channel matrix $\hat{\mathbf{H}}_{\setminus t} = (\hat{\mathbf{h}}_{1,\setminus t}, \dots, \hat{\mathbf{h}}_{K,\setminus t})$ and an AWGN vector with covariance $(\zeta_t + N_0) \mathbf{I}_N$. In order to obtain the LMMSE estimator of $x_{k,t}$, we approximate the a priori distributions of the other data symbols $x_{k',t}$ by proper complex Gaussian distributions with mean $\hat{x}_{k',t}$ and covariance $\sigma_{k',t}^2$ for all $k' \neq k$, whereas the a priori distribution of $x_{k,t}$ is approximated by the CSCG distribution with unit variance. As shown in [33], the approximate a posteriori pdf of $x_{k,t}$ is evaluated as

$$p(x_{k,t} | \mathbf{y}_t, \hat{\mathbf{H}}_{\setminus t}, \{\hat{x}_{k',t}\}) = \frac{1}{\pi \zeta_{k,t}^{\text{dem}}} \exp \left(- \frac{|x_{k,t} - \bar{x}_{k,t}|^2}{\zeta_{k,t}^{\text{dem}}} \right), \quad (20)$$

where the LMMSE estimate $\bar{x}_{k,t}$ and its mean-squared error (MSE) $\zeta_{k,t}^{\text{dem}}$ are given by

$$\bar{x}_{k,t} = \zeta_{k,t}^{\text{dem}} \hat{\mathbf{h}}_{k,\setminus t}^H \mathbf{\Xi}_{\setminus k,t}^{\text{dem}} \left(\mathbf{y}_t - \sum_{k' \neq k} \hat{\mathbf{h}}_{k',\setminus t} \hat{x}_{k',t} \right), \quad (21)$$

$$\zeta_{k,t}^{\text{dem}} = \left(1 + \hat{\mathbf{h}}_{k,\setminus t}^H \mathbf{\Xi}_{\setminus k,t}^{\text{dem}} \hat{\mathbf{h}}_{k,\setminus t} \right)^{-1}, \quad (22)$$

respectively. In these expressions, $\mathbf{\Xi}_{\setminus k,t}^{\text{dem}}$ is defined as

$$\mathbf{\Xi}_{\setminus k,t}^{\text{dem}} = \left((N_0 + \zeta_t) \mathbf{I}_N + \sum_{k' \neq k} \sigma_{k',t}^2 \hat{\mathbf{h}}_{k',\setminus t} \hat{\mathbf{h}}_{k',\setminus t}^H \right)^{-1}. \quad (23)$$

In (20), we have omitted the conditioning with respect to ζ_t and $\{\sigma_{k',t}^2 : k' \neq k\}$. Since (19) is independent of the index k , it is possible to calculate (23) for all k efficiently, by using the same method as in Appendix A.

Remark 2. In order to reduce the complexity of the demodulator, we have used the feedback information $\hat{x}_{k,t}$ and $\sigma_{k,t}^2$ about the k th data symbol $x_{k,t}$ in the definition of (19). This violates the update rule of BP in which the feedback information about $x_{k,t}$ should not be used in its detection. However, this influence will be shown to vanish in the large-system limit. As a result, the proposed LMMSE demodulator in that limit reduces to the true LMMSE demodulator in which $\hat{x}_{k,t}$ and $\sigma_{k,t}^2$ in (19) are replaced by 0 and 1, respectively.

E. Soft Demapper

The soft demapper sends the LLR L_q^{dem} of the q th bit c_q for the data symbol $x_{k,t}$ to the decoder for $q = 1, \dots, Q$. The extrinsic probability $P^{\text{dem}}(c_q)$ of c_q is given by

$$P^{\text{dem}}(c_q) \propto \sum_{\{c_{q'}\}_{c_q}} p(x_{k,t} = F(\{c_{q'}\}) | \mathbf{y}_t, \hat{\mathbf{H}}_{\setminus t}, \{\hat{x}_{k',t}\}) \cdot \prod_{q' \neq q} P^{\text{dec}}(c_{q'}). \quad (24)$$

In (24), F denotes the mapping function, and the pdf $p(x_{k,t} | \mathbf{y}_t, \hat{\mathbf{H}}_{\setminus t}, \{\hat{x}_{k',t}\})$ sent from the demodulator is given by (20). Furthermore, $P^{\text{dec}}(c_{q'})$ represents the a priori probability (7). The summation in (24) is taken over all possible binary sequences (c_1, \dots, c_Q) with c_q fixed. Then, the extrinsic LLR L_q^{dem} to be fed forward is defined as

$$L_q^{\text{dem}} = \ln \frac{P^{\text{dem}}(c_q = 0)}{P^{\text{dem}}(c_q = 1)}. \quad (25)$$

F. Sliding-Window Schedule

The performance of the iterative CE-MUDD depends on message-passing schedules. We use a sliding-window (SW) schedule with a window size of W_{SW} sections. The decoding window runs in the ascending order of sections $l = 0, \dots, L-1$, because of the termination structure (3) of the SC LDPC code. In stage $l \in [0 : L - W_{\text{SW}}]$ of the SW decoding, W_{SW} codewords in sections $[l : l + W_{\text{SW}})$ are decoded on the basis of the decoding results in the preceding stages and of the received signals in the $(W_{\text{SW}} + 2W)$ sections $[l - W : l +$

$W_{\text{SW}} + W$), associated with the W_{SW} codewords, while the received signals in the sections $[l - W : L)$ are used for the last stages $l \in [L - W_{\text{SW}} - W : L - W_{\text{SW}}]$. Thus, the decoding latency is $O((W_{\text{SW}} + 2W)M)$, and independent of the number L of sections.

In each stage, we regard the four parts separated by the interleaver and the deinterleaver—shown in Fig. 4—as one effective demodulator *without* inner iterations. Thus, messages are updated between the BP decoder with inner iterations and the effective demodulator. We use the parallel schedule in the outer iterations between the effective demodulator and the decoder. In the parallel schedule, all data symbols in $(W_{\text{SW}} + 2W)$ sections are demodulated and then fed forward to the decoder. The decoder use the received messages to perform iterative decoding of the W_{SW} codewords on the basis of on-demand check node updating schedule [17] with inner iterations I , which is the total number of updating the message of each variable node in one decoding. Thus, the total number of updating each variable node is IJ in each stage of the SW schedule, in which J is the number of outer iterations between the effective demodulator and the decoder in each stage. Furthermore, the corresponding total number is equal to $W_{\text{SW}}IJ$ in one CE-MUDD for the bulk region of sections.

In one round of stage l for the SW decoding with the on-demand check node updating schedule, the variable nodes in sections l' are updated in the ascending order $l' = l, \dots, l + W_{\text{SW}} - 1$. All variable nodes in each section are updated simultaneously, after updating all check nodes that are directly connected to the variable nodes. Such I rounds are repeated in each stage of the BP decoder. See [17] for the details.

IV. DENSITY EVOLUTION ANALYSIS

A. Large System Analysis

The DE analysis is presented in the large-system limit after taking the long code-length limit $M \rightarrow \infty$. In the large-system limit, N , K , T , and T_{tr} tend to infinity at the same rate. We note that each codeword is transmitted over many fading blocks since M tends to infinity with coherence time T fixed. In this sense, the limits in this paper correspond to fast fading.

As noted in Remark 1, we assume that the noise value N_0 postulated in the channel estimator is equal to the true one N_0 in the DE analysis. We evaluate the average performance over all possible information bits, the (d_v, d_c, L) ensemble of SC LDPC codes, and the (M, L, W, Q) ensemble of STC BICM. For given information bits, an SC LDPC code, and STC BICM, each soft decision $\hat{x}_{k,t}$ should be biased toward the true data symbol $x_{k,t}$ as the iteration proceeds. However, the average $\mathbb{E}[\hat{x}_{k,t}]$ over all possible randomness is equal to zero since the data symbol $x_{k,t}$ should appear on the constellation points \mathcal{C} uniformly. Furthermore, the assumption of random bit-interleaving implies that the soft decisions and the a priori variances $\{\hat{x}_{k,t}, \sigma_{k,t}^2\}$ are independent for all k and t in the limit $M \rightarrow \infty$. We use these asymptotic properties to analyze the channel estimator and the demodulator.

B. LMMSE Channel Estimator

We first present the large-system analysis for the LMMSE channel estimator. Let us focus on symbol period t within

a fading block in section l . Let $\xi_{\setminus t}(l)$ denote the average MSE of the LMMSE channel estimation in section l over the codewords and the ensemble of STC BICM,

$$\xi_{\setminus t}(l) = \mathbb{E} \left[\text{Tr}(\Xi_{\setminus t}^{\text{ch}}) \right], \quad (26)$$

where $\Xi_{\setminus t}^{\text{ch}}$ is given by (17). We note that (26) is $O(1)$ in the large-system limit. The average MSE is characterized by the average squared soft decision $\mathbb{E}[|\hat{x}_{k',t'}|^2]$. From the construction of the STC BICM, $\mathbb{E}[|\hat{x}_{k',t'}|^2]$ in section l is given by

$$\hat{x}_{\text{dec}}^2(l) = \frac{1}{2W+1} \sum_{w=-W}^W \mathbb{E} \left[|\hat{x}(\mathcal{L}_{f_l(w)}^{\text{dec}})|^2 \right], \quad (27)$$

with

$$f_l(w) = \begin{cases} l+w & \text{for } l+w \in [-W : L) \\ l & \text{otherwise.} \end{cases} \quad (28)$$

In (27), $\mathcal{L}_l^{\text{dec}}$ denotes the set of Q independent and identically distributed (i.i.d.) random variables that represent the LLRs fed back from the decoder in section l . Furthermore, the soft decision $\hat{x}(\mathcal{L}^{\text{dec}})$ is the mean of the data symbol with respect to the a priori distribution (8) defined via the LLRs \mathcal{L}^{dec} . See Examples 1 and 2 for QPSK and 16 QAM, respectively. The expectation in (27) is taken over the distribution of the LLRs $\mathcal{L}_{f_l(w)}^{\text{dec}}$, which will be analyzed shortly.

It is shown that the average MSE (26) is given via the following function in the large-system limit:

$$\xi(\sigma_{\text{tr}}^2, \sigma_c^2; l) = \left(1 + \frac{T_{\text{tr}}}{K\sigma_{\text{tr}}^2} + \frac{(T - T_{\text{tr}} - 1)\hat{x}_{\text{dec}}^2(l)}{K\sigma_c^2} \right)^{-1}. \quad (29)$$

See [43] for the operational meaning of (29).

Proposition 1. *Focus on a fading block in section l . Suppose that $\hat{x}_{\text{dec}}^2(l)$ is given by (27) via the feedback information from the decoder in an iteration round, and that $(\sigma_{\text{tr}}^2, \sigma_c^2)$ is the solution to the coupled fixed-point (FP) equations*

$$\sigma_{\text{tr}}^2 = N_0 + \xi(\sigma_{\text{tr}}^2, \sigma_c^2; l), \quad (30)$$

$$\sigma_c^2 = N_0 + 1 - \hat{x}_{\text{dec}}^2(l) + \hat{x}_{\text{dec}}^2(l)\xi(\sigma_{\text{tr}}^2, \sigma_c^2; l), \quad (31)$$

where $\hat{x}_{\text{dec}}^2(l)$ and $\xi(\sigma_{\text{tr}}^2, \sigma_c^2; l)$ are given by (27) and (29), respectively. Then, the difference between the two MSEs (26) and (29) converges to zero in the large-system limit after taking the limit $M \rightarrow \infty$.

Proof: See Appendix B. ■

The quantity (29) has a well-defined limit as K , T , and T_{tr} tend to infinity with their ratios K/T and T_{tr}/T kept constant. In this paper, (29) is used as an approximation of the average MSE (26) for finite-sized systems. It was numerically demonstrated in [43] that (29) is a good approximation for small MIMO systems.

C. LMMSE Demodulator

We next present the large-system analysis for the LMMSE demodulator. Let us define the equivalent channel between the

mapper and the demapper as

$$p(\tilde{x}_{k,t}|x_{k,t}, \{\hat{x}_{k',t}\}) = \mathbb{E}_{\mathbf{H}, \hat{\mathbf{H}}_{\setminus t}} \left[\int p(\mathbf{y}_t | \mathbf{H}, x_{k,t}) \cdot p(x_{k,t} = \tilde{x}_{k,t} | \mathbf{y}_t, \hat{\mathbf{H}}_{\setminus t}, \{\hat{x}_{k',t}\}) d\mathbf{y}_t \right]. \quad (32)$$

In (32), the pdf $p(\mathbf{y}_t | \mathbf{H}, x_{k,t})$ represents the MIMO channel (1) in symbol period t marginalized over the data symbols $\{x_{k',t} : k' \neq k\}$ with the exception of $x_{k,t}$. The a posteriori pdf $p(x_{k,t} | \mathbf{y}_t, \hat{\mathbf{H}}_{\setminus t}, \{\hat{x}_{k',t}\})$ is given by (20). The expectation $\mathbb{E}_{\mathbf{H}, \hat{\mathbf{H}}_{\setminus t}}[\cdot]$ is taken over the joint distribution of the channel matrix \mathbf{H} and its LMMSE estimate (16) induced from (13), as well as over all possible codewords and interleavers. It is shown that the equivalent channel converges to that for an interference-free AWGN channel in the large-system limit.

We focus on section l , and define the AWGN channel as

$$z_l = \sqrt{1 - \xi(\sigma_{\text{tr}}^2, \sigma_c^2; l)} x_l + n_l, \quad n_l \sim \mathcal{CN}(0, \sigma_{\text{dem}}^2(l)), \quad (33)$$

with x_l denoting the input symbol for section l . In (33), $\xi(\sigma_{\text{tr}}^2, \sigma_c^2; l)$ defined by (29) is given via the solution to the coupled FP equations (30) and (31). The equivalent channel for the AWGN channel (33) is defined as

$$p(\tilde{x}_l | x_l) = \int p(x_l = \tilde{x}_l | z_l) p(z_l | x_l) dz_l. \quad (34)$$

In (34), $p(z_l | x_l)$ denotes the AWGN channel (33). Furthermore, $p(x_l | z_l)$ is the a posteriori pdf of the input symbol with the Gaussian a priori pdf $x_l \sim \mathcal{CN}(0, 1)$.

Proposition 2. *Focus on section l . Suppose that $\xi_l \equiv \xi(\sigma_{\text{tr}}^2, \sigma_c^2; l)$ defined by (29) is given via the solution to the coupled FP equations (30) and (31) in Proposition 1, and that $\sigma_{\text{dem}}^2(l)$ is the solution σ_{dem}^2 to the following FP equation*

$$\sigma_{\text{dem}}^2 = \frac{K}{N} \left\{ N_0 + \xi_l + \frac{1 - \xi_l}{2W + 1} \sum_{w=-W}^W \text{MSE}_{f_l(w)}(\sigma_{\text{dem}}^2) \right\}, \quad (35)$$

with

$$\text{MSE}_l(\sigma_{\text{dem}}^2) = \mathbb{E} \left[\frac{\sigma^2(\mathcal{L}_l^{\text{dec}}) \sigma_{\text{dem}}^2}{(1 - \xi_l) \sigma^2(\mathcal{L}_l^{\text{dec}}) + \sigma_{\text{dem}}^2} \right]. \quad (36)$$

In (35) and (36), $f_l(w)$ is given by (28). Furthermore, $\sigma^2(\mathcal{L}_l^{\text{dec}})$ is the variance of the data symbol that has the a priori distribution (8) defined via the LLRs $\mathcal{L}_l^{\text{dec}}$. Then, the equivalent channel (32) converges to (34) for the AWGN channel in the large-system limit after taking the long code-length limit, i.e., for almost all realizations of $\{\hat{x}_{k',t}\}$

$$p(\tilde{x}_{k,t} | x_{k,t}, \{\hat{x}_{k',t}\}) - p(\tilde{x}_l = \tilde{x}_{k,t} | x_l = x_{k,t}) \rightarrow 0. \quad (37)$$

Proof: Repeat the derivation of Proposition 1. ■

The function $\sigma^2(\mathcal{L}^{\text{dec}})$ is given in Examples 1 and 2 for QPSK and 16 QAM, respectively. Proposition 2 implies that the equivalent channel between the mapper and the demapper reduces to the AWGN channel in the large-system limit. Thus, we can apply the DE analysis of conventional BICM [56] to evaluating the expectation in (36) over the LLRs $\{\mathcal{L}_l^{\text{dec}}\}$.

D. Soft Demapper

We focus on the soft demapper in section l , and analyze the LLR distribution that is fed forward to the decoders in sections $l' = f_l(w)$, given by (28), for $w = -W, \dots, W$. In Proposition 2 we have shown that the equivalent channel for section l reduces to the complex AWGN channel (33). Let $P_{l \rightarrow l'}^{\text{dem}}(c_q)$ denote the extrinsic probability of the q th bit c_q for the data symbol x_l ,

$$P_{l \rightarrow l'}^{\text{dem}}(c_q) \propto \sum_{\{c_{q'}\} \setminus c_q} p(z_l | x_l = F(\{c_{q'}\})) \prod_{q' \neq q} P_{l'}^{\text{dec}}(c_{q'}). \quad (38)$$

In (38), $P_{l'}^{\text{dec}}(c_{q'})$ denotes the a priori probability fed back from the l' th decoder, which is defined in the same manner as in (7). Furthermore, the pdf $p(z_l | x_l)$ represents the AWGN channel (33) with F denoting the mapping function. The extrinsic probability (38) sent to the l' th decoder depends only on the feedback information from the same decoder, since each data symbol originates from the same codeword.

From Proposition 2, the LLRs (25) sent from the demapper in section l to the l' th decoder are statistically equivalent to the LLRs

$$L_{l \rightarrow l', q}^{\text{dem}} = \ln \frac{P_{l \rightarrow l'}^{\text{dem}}(c_q = 0)}{P_{l \rightarrow l'}^{\text{dem}}(c_q = 1)}, \quad q = 1, \dots, Q, \quad (39)$$

in the large-system limit. The RHS is a random variable that depends on the received signal z_l and the LLRs fed back from the l' th decoder.

The distributions of the LLRs (39) are Gaussian-distributed for QPSK ($Q = 2$). Furthermore, it is possible to estimate them via numerical sampling, although the exact distributions for $Q > 2$ have intractable expressions. Since the use of Gray mapping has been assumed, the LLRs (39) are classified into statistically equivalent two groups for the in-phase and quadrature components. The distribution sent to the decoder is the mixture of the distributions of the $Q/2$ LLRs in each group. In order to simplify the analysis of the demapper, we approximate the mixture distribution by a Gaussian distribution. Under the Gaussian approximation, it is sufficient to estimate the average entropy $h_{l \rightarrow l'}^{\text{dem} \rightarrow \text{dec}}$ of (38) over all q via numerical sampling.

The Gaussian approximation might be too simple to characterize the properties of mixture distributions for $Q > 2$, although it is a popular approximation in the literature. It is beyond the scope of this paper to construct more sophisticated approximations.

Under the Gaussian approximation [38], the LLR distribution is approximated by the real Gaussian distribution with mean $m_{l \rightarrow l'}^{\text{dem} \rightarrow \text{dec}}$ and variance $2m_{l \rightarrow l'}^{\text{dem} \rightarrow \text{dec}}$ when the corresponding true bit is zero. Otherwise, it is approximated by $\mathcal{N}(-m_{l \rightarrow l'}^{\text{dem} \rightarrow \text{dec}}, 2m_{l \rightarrow l'}^{\text{dem} \rightarrow \text{dec}})$. We define the function $h_{l \rightarrow l'}^{\text{dem} \rightarrow \text{dec}} = \psi(m_{l \rightarrow l'}^{\text{dem} \rightarrow \text{dec}})$ to specify the relationship between the mean $m_{l \rightarrow l'}^{\text{dem} \rightarrow \text{dec}}$ and the entropy $h_{l \rightarrow l'}^{\text{dem} \rightarrow \text{dec}}$.

$$\psi(m) = \int_{\mathbb{R}} S \left(\frac{e^{L/2}}{e^{L/2} + e^{-L/2}} \right) \frac{1}{\sqrt{4\pi m}} e^{-\frac{(L-m)^2}{4m}} dL, \quad (40)$$

where $S(p)$ denotes the binary entropy function

$$S(p) = -p \log_2 p - (1-p) \log_2 (1-p). \quad (41)$$

The function $\psi(m)$ is regarded as the average entropy of a binary random variable characterized by a Gaussian-distributed LLR L with mean m and variance $2m$. Since (40) is monotonically decreasing, the inverse function ψ^{-1} exists.

E. BP Decoder

We shall analyze the BP decoder for the (d_v, d_c, L) ensemble of SC LDPC codes under the Gaussian approximation. We have shown that the analysis of the l th decoder reduces to that of the decoder with the information $\{h_{l' \rightarrow l}^{\text{dem} \rightarrow \text{dec}} : l' = f_l(w), w \in [-W : W]\}$ from the demapper.

Without loss of generality, transmission of all-zero codewords is assumed. We focus on section l , and analyze the variable-to-check message update. Suppose that the variable nodes in section l have received the entropy $h_{l+w \rightarrow l}^{c \rightarrow v}$ from the check nodes in section $l+w$ for $w \in [0 : d_v]$ in an inner iteration. We approximate the pdf of the LLRs emitted from the check nodes by the Gaussian pdf with mean $\psi^{-1}(h_{l+w \rightarrow l}^{c \rightarrow v})$ and variance $2\psi^{-1}(h_{l+w \rightarrow l}^{c \rightarrow v})$. From the construction of the (d_v, d_c, L) ensemble of protograph-based SC LDPC codes, each variable node in section l emits the sum of LLRs sent from a demapper and $d_v - 1$ check nodes. Thus, the average entropy $h_{l \rightarrow l+w}^{v \rightarrow c}$ passed from the variable nodes in section l to the check nodes in section $l+w$ is given by

$$h_{l \rightarrow l+w}^{v \rightarrow c} = \frac{1}{2W+1} \sum_{w'=-W}^W \psi \left(\psi^{-1}(h_{f_l(w') \rightarrow l}^{\text{dem} \rightarrow \text{dec}}) + \sum_{w'' \in [0: d_v], w'' \neq w} \psi^{-1}(h_{l+w'' \rightarrow l}^{c \rightarrow v}) \right). \quad (42)$$

In (42), ψ^{-1} denotes the inverse function of ψ given by (40). Furthermore, $h_{f_l(w') \rightarrow l}^{\text{dem} \rightarrow \text{dec}}$ denotes the entropy sent from the demapper in section $f_l(w')$, given by (28), to the variable nodes in section l .

We next analyze the check-to-variable message update. Assume that the check nodes in section l have received the entropy $h_{l-w \rightarrow l}^{v \rightarrow c}$ from the variable nodes in section $l-w$ for $w \in [0 : d_v]$. We approximate the distribution of the LLRs emitted from the variable nodes by $\mathcal{N}(\psi^{-1}(h_{l-w \rightarrow l}^{v \rightarrow c}), 2\psi^{-1}(h_{l-w \rightarrow l}^{v \rightarrow c}))$. In order to calculate the entropy $h_{l \rightarrow l-w}^{c \rightarrow v}$, we use the duality between variable nodes with entropy h and check nodes with entropy $(1-h)$ [57]. Exchanging the roles of variable nodes and check nodes, and repeating the derivation of (42), we obtain

$$h_{l \rightarrow l-w}^{c \rightarrow v} = 1 - \psi \left(\left(\frac{d_c}{d_v} - 1 \right) \psi^{-1}(1 - h_{l-w \rightarrow l}^{v \rightarrow c}) + \frac{d_c}{d_v} \sum_{w' \in [0: d_v], w' \neq w} \psi^{-1}(1 - h_{l-w' \rightarrow l}^{v \rightarrow c}) \right), \quad (43)$$

with $h_{l-w' \rightarrow l}^{v \rightarrow c} = 0$ for $l-w' < 0$.

Finally, we analyze the entropy emitted from the decoder in section l . Suppose that the variable nodes in section l have received the entropy $h_{l+w \rightarrow l}^{c \rightarrow v}$ from the check nodes in section $l+w$ for $w \in [0 : d_v]$ in the last inner iteration. The

entropy $h_l^{\text{dec} \rightarrow \text{dem}}$ for the LLRs emitted from the decoder in section l is given by

$$h_l^{\text{dec} \rightarrow \text{dem}} = \psi \left(\sum_{w=0}^{d_v-1} \psi^{-1}(h_{l+w \rightarrow l}^{c \rightarrow v}) \right). \quad (44)$$

Similarly, the entropy h_l^{dec} of the a posteriori LLRs in section l is given by

$$h_l^{\text{dec}} = \frac{1}{2W+1} \sum_{w=-W}^W \psi \left(\psi^{-1}(h_{f_l(w) \rightarrow l}^{\text{dem} \rightarrow \text{dec}}) + \sum_{w'=0}^{d_v-1} \psi^{-1}(h_{l+w' \rightarrow l}^{c \rightarrow v}) \right), \quad (45)$$

which is associated with the decoding performance.

The symmetry of linear codes implies that the entropy (44) is independent of the realizations of codewords. Thus, the pdf $p_l^{\text{dec}}(L)$ of the LLRs emitted from the decoder in section l is approximated by the mixture Gaussian pdf

$$p_l^{\text{dec}}(L) = \frac{1}{2} \sum_{a=\pm 1} p_G(L; am_l^{\text{dec} \rightarrow \text{dem}}, 2m_l^{\text{dec} \rightarrow \text{dem}}), \quad (46)$$

with $m_l^{\text{dec} \rightarrow \text{dem}} = \psi^{-1}(h_l^{\text{dec} \rightarrow \text{dem}})$. In (46), $p_G(\cdot : m, \sigma^2)$ denotes the real Gaussian pdf with mean m and variance σ^2 .

We summarize the DE analysis for the inner iteration in stage l' of the SW decoding with the on-demand check node updating schedule.

- 1) Let $j = 1$. For all $l \in [l' : l' + W_{\text{SW}} + d_v - 2]$ and $w \in [0 : d_v]$, let $h_{l \rightarrow l-w}^{c \rightarrow v} = 1$ if $h_{l \rightarrow l-w}^{c \rightarrow v}$ is not initialized. Otherwise, use the current value. For all $l \in [l' : l' + W_{\text{SW}})$ and $w \in [0 : d_v]$, update the entropy $h_{l \rightarrow l+w}^{v \rightarrow c}$ with (42).
- 2) Repeat the following in the order $l = l', \dots, l' + W_{\text{SW}} - 1$:
 - Update $h_{l+w \rightarrow l}^{c \rightarrow v}$ with (43) for all $w \in [0 : d_v]$.
 - Update $h_{l \rightarrow l+w}^{v \rightarrow c}$ with (42) for all $w \in [0 : d_v]$.
- 3) Let $j := j + 1$ and go back to Step 2) if j is smaller than the total number J of inner iterations. Otherwise, output the entropy $h_l^{\text{dec} \rightarrow \text{dem}}$ given by (44) for all $l \in [l' : l' + W_{\text{SW}})$.

F. Density Evolution for Outer Iteration

The DE analysis for the outer iteration is summarized for the SW schedule.

- Initialize $h_l^{\text{dec} \rightarrow \text{dem}} = 0$ for $l \in [-W : 0)$ and $h_l^{\text{dec} \rightarrow \text{dem}} = 1$ for $l \in [0 : L)$.
- Repeat the following in the order $l' = 0, \dots, L - W_{\text{SW}}$:
 - 1) Let $i = 1$.
 - 2) For all $l \in [l' - W : l' + W_{\text{SW}} + W)$, let $\hat{x}_{\text{dec}}^2(l) = 0$ if $h_l^{\text{dec} \rightarrow \text{dem}} = 1$. Otherwise, evaluate $\hat{x}_{\text{dec}}^2(l)$ given by (27) via the LLR distribution (46).
 - 3) Calculate the asymptotic MSE (29) based on Proposition 1, and then solve the FP equation (35) in Proposition 2 with the LLR distribution (46) for all $l \in [l' - W : l' + W_{\text{SW}} + W)$.
 - 4) Estimate the average entropy $h_{l \rightarrow f_l(w)}^{\text{dem} \rightarrow \text{dec}}$ for all $l \in [l' - W : l' + W_{\text{SW}} + W)$ and $w \in [-W : W]$, via

numerical sampling of the LLRs (39) based on the LLR distributions (46) and the AWGN channel (33) with SNR $(1 - \xi_l)/\sigma_{\text{dem}}^2(l)$.

- 5) Calculate the entropy $h_l^{\text{dec} \rightarrow \text{dem}}$ given by (44) for all $l \in [l' : l' + W_{\text{SW}}]$, by performing the DE analysis for the inner iteration, presented in Section IV-E.
- 6) Let $i := i + 1$ and go back to Step 2) if i is smaller than the total number I of outer iterations. Otherwise, output the entropy h_l^{dec} given by (45).

We shall define the threshold for the iterative CE-MUDD. When the window size W_{SW} tends to infinity, there exists some threshold $\rho > 0$ such that the entropy h_l^{dec} of the a posteriori LLRs converges to zero for all SNRs $1/N_0 > \rho$, whereas h_l^{dec} is strictly positive in some section l for all $1/N_0 < \rho$. However, the entropy h_l^{dec} may not converge to zero [17], as long as the window size W_{SW} is finite. In other words, the average bit error ratio (BER) may not tend to zero. In order to present a formal definition of the threshold for the SW schedule, we define the average BER in section l as

$$p_{\text{BER}}(h_l^{\text{dec}}) = Q\left(\sqrt{\frac{\psi^{-1}(h_l^{\text{dec}})}{2}}\right), \quad (47)$$

with $Q(\cdot)$ denoting the Q-function. In (47), the entropy h_l^{dec} is given by (45).

Definition 2. For given $\epsilon \geq 0$, the threshold ρ_{BP} for the iterative CE-MUDD is defined as the infimum of the SNR ρ such that, after I outer iterations, the average BERs $p_{\text{BER}}(h_l^{\text{dec}})$ converge to values below ϵ for all $1/N_0 > \rho$ and $l \in [0 : L]$.

The iterative CE-MUDD can achieve an average BER below ϵ in the large-system limit after taking $M \rightarrow \infty$ if and only if the SNR $1/N_0$ is larger than the threshold. When the window size W_{SW} tends to infinity, the iterative CE-MUDD can achieve zero average BER for all SNRs $1/N_0$ greater than a threshold for $\epsilon = 0$. When the window size W_{SW} is finite, on the other hand, the average BER achieved by the iterative CE-MUDD decreases toward zero very quickly, as the SNR grows from a threshold for strictly positive $\epsilon > 0$. However, it is open whether there exists a finite threshold ρ_{BP} such that zero average BER is achieved for all $1/N_0 > \rho_{\text{BP}}$ when a finite window size W_{SW} is used.

V. NUMERICAL RESULTS

A. Density Evolution

In all numerical results, we consider 6×6 MIMO systems over Rayleigh block-fading channels with coherence time $T = 64$. As noted in Remark 1, the noise variance \tilde{N}_0 postulated in the channel estimator is assumed to be equal to the true one N_0 in the DE analysis, whereas a mismatched value $\tilde{N}_0 \neq N_0$ may be used in numerical simulations.

We compare four systems in terms of the decoding threshold, shown in Table I. One system consists of $(3, 6)$ LDPC coding and conventional BICM with $W = 0$, and is called a conventional system. The BP algorithm is assumed in decoding. In a second system, the STC BICM with $W \geq 1$ is used instead of the conventional BICM. Since the performance is poor in sections at the right end, we consider STC BICM with

TABLE I
FOUR SYSTEMS COMPARED IN THIS PAPER.

	coding	BICM
Conventional system	LDPC	$W = 0$
Coupled system in BICM	LDPC	$W \geq 1$
Coupled system in coding	SC LDPC	$W = 0$
Coupled system in both coding and BICM	SC LDPC	$W \geq 1$

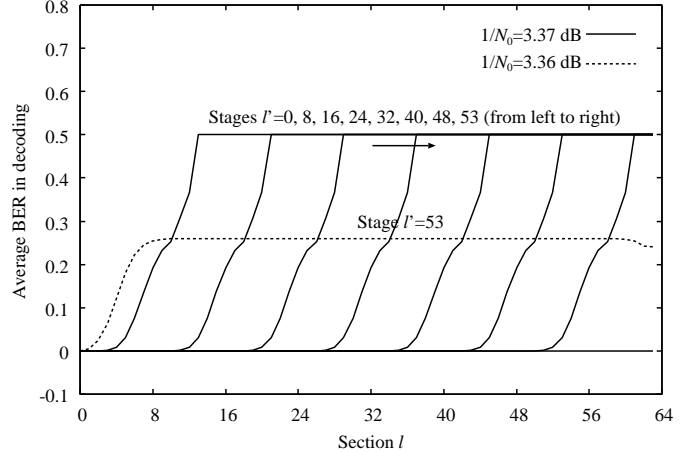


Fig. 5. Average BER in decoding versus section l for $(3, 6, 64)$ SC LDPC coding, $(\infty, 64, 1, 2)$ STC BICM with QPSK, the SW schedule with window size $W_{\text{SW}} = 11$ and the numbers $J = \infty$ and $I = \infty$ of inner and outer iterations, and 6×6 block-fading MIMO with coherence time $T = 64$ and the number of pilots $T_{\text{tr}} = 6$.

$2(L + W)$ sections in which known words are sent in sections l at both ends for $l \in [-W : 0)$ and $l \in [2L : 2L + W)$. In the SW decoding, two decoding windows run from both ends toward the center. The system corresponds to those in [34], [43], and has the same overall rate as (6) for the other systems. We refer to this STC BICM as (M, L, W, Q) both-side STC BICM or simply as (M, L, W, Q) STC BICM.

A third system is constructed from $(3, 6, L)$ SC LDPC coding (3) with efficient termination for encoding [54] and from the conventional BICM with $W = 0$. The third system is called the coupled system in coding, whereas the second system is referred to as the coupled system in BICM. The third system was investigated for the AWGN channel in [58]. In the last system, coupling is introduced for both coding and BICM. The system consists of $(3, 6, L)$ SC LDPC coding (3) and (M, L, W, Q) one-side STC BICM. Thus, we referred to the last system as the coupled system in both coding and BICM.

We first present the dynamics of the SW decoding as the decoding stage proceeds. Figure 5 shows the average BER in decoding versus section l for the coupled system in both coding and BICM with QPSK. The decoding proceeds from left to right, and eventually almost zero average BER is accomplished for $1/N_0 = 3.37$ dB, whereas the average BER is distinct from zero for $1/N_0 = 3.36$ dB.

Figure 6 shows the extrinsic information transfer (EXIT) chart for the underlying $(3, 6)$ LDPC coding and the conventional BICM with QPSK. The SNR $1/N_0 = 5.98$ dB is approximately equal to the threshold for the combination of the conventional BICM and the $(3, 6)$ LDPC coding under

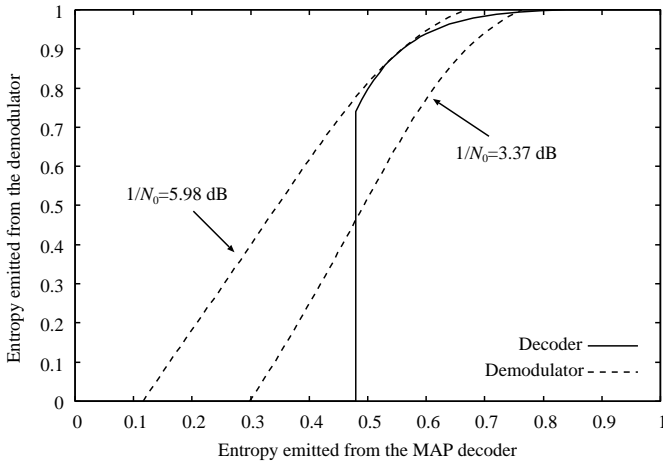


Fig. 6. EXIT chart for (3, 6) LDPC coding under the MAP decoding, conventional BICM with QPSK ($W = 0$), and 6×6 block-fading MIMO with coherence time $T = 64$ and the number of pilots $T_{tr} = 6$.

TABLE II

THRESHOLDS FOR (3, 6) LDPC (TOP) AND (3, 6, ∞) SC LDPC (BOTTOM) CODING. WE USED $(\infty, \infty, W, 2)$ STC BICM WITH QPSK, THE SW SCHEDULE WITH INFINITE WINDOW SIZE $W_{SW} = \infty$ AND THE NUMBER OF OUTER ITERATIONS $I = \infty$, THE BER REQUIREMENT $\epsilon = 0$, AND 6×6 BLOCK-FADING MIMO WITH COHERENCE TIME $T = 64$.

	$T_{tr} = 0$	$T_{tr} = 2$	$T_{tr} = 4$	$T_{tr} = 6$	Perfect CSI
$W = 0$	∞ dB	17.3 dB	7.40 dB	5.98 dB	2.94 dB
	∞ dB	3.76 dB	3.54 dB	3.37 dB	1.69 dB
$W = 1$	5.39 dB	4.87 dB	4.50 dB	4.24 dB	2.36 dB
	4.04 dB	3.76 dB	3.54 dB	3.37 dB	1.67 dB
$W = 2$	5.04 dB	4.62 dB	4.31 dB	4.07 dB	2.28 dB
	4.04 dB	3.76 dB	3.54 dB	3.36 dB	1.66 dB

the MAP decoding, since the two EXIT curves have the unique intersection at (0.116, 0). Thus, the threshold for the conventional system would be worse than 5.98 dB, since the BP decoding is actually used instead of the MAP decoding. As shown in Fig. 5, on the other hand, the SNR $1/N_0 = 3.37$ dB is achievable by the coupled system in both coding and BICM under the SW decoding. Thus, coupling can provide a performance gain of 2.61 dB. We observe that the two EXIT curves have three points of intersection at the SNR $1/N_0 = 3.37$ dB. If coupling were not used, the system would converge to the top FP that has the maximum entropy among the three FPs. Coupling allows the system to converge toward the bottom FP with zero entropy even when there are multiple FPs.

Table II lists the thresholds of the iterative CE-MUDD for the four systems with QPSK. Note that the overall rate (6) is equal to $R = (1 - T_{tr}/T)QKr$, with the design rate $r = 1/2$ in coding, for all systems, since the limit $L \rightarrow \infty$ is assumed. Thus, each column in the table contains systems with the same rate R . We simulated the numbers of inner iterations $J = 1$ and $J = \infty$, and found that the thresholds are the same as each other for the two cases. Thus, the thresholds are independent of the number of inner iterations J , as long as the number of outer iterations $I = \infty$ is considered. From Definition 2, the decoder can achieve the BER requirement

TABLE III

THRESHOLDS FOR (3, 6) LDPC (TOP) AND (3, 6, ∞) SC LDPC (BOTTOM) CODING. THE OTHER CONDITIONS ARE THE SAME AS IN TABLE II, WITH THE EXCEPTION OF $(\infty, \infty, W, 4)$ STC BICM WITH 16 QAM.

	$T_{tr} = 0$	$T_{tr} = 2$	$T_{tr} = 4$	$T_{tr} = 6$	Perfect CSI
$W = 0$	∞ dB	∞ dB	∞ dB	16.3 dB	10.8 dB
	∞ dB	13.2 dB	11.9 dB	11.1 dB	8.2 dB
$W = 1$	19.5 dB	15.2 dB	13.4 dB	12.2 dB	8.8 dB
	13.9 dB	12.5 dB	11.5 dB	10.8 dB	8.0 dB
$W = 2$	16.3 dB	13.8 dB	12.4 dB	11.6 dB	8.6 dB
	13.3 dB	12.1 dB	11.2 dB	10.6 dB	7.9 dB

TABLE IV

THRESHOLDS FOR (3, 6) LDPC (TOP) AND (3, 6, ∞) SC LDPC (BOTTOM) CODING. THE OTHER CONDITIONS ARE THE SAME AS IN TABLE II, WITH THE EXCEPTION OF $(\infty, \infty, W, 6)$ STC BICM WITH 64 QAM.

	$T_{tr} = 4$	$T_{tr} = 8$	$T_{tr} = 12$	$T_{tr} = 16$	Perfect CSI
$W = 0$	∞ dB	23.8 dB	21.2 dB	20.3 dB	18.3 dB
	∞ dB	17.7 dB	16.5 dB	16.0 dB	14.4 dB
$W = 1$	26.3 dB	18.0 dB	16.7 dB	16.1 dB	14.4 dB
	21.4 dB	17.1 dB	16.0 dB	15.5 dB	13.9 dB
$W = 2$	22.7 dB	17.3 dB	16.1 dB	15.6 dB	14.0 dB
	20.2 dB	16.5 dB	15.5 dB	15.0 dB	13.5 dB

$\epsilon = 0$ for all sections if and only if the SNR $1/N_0$ is larger than the corresponding threshold. Infinite thresholds imply that the average BER cannot tend to zero for $N_0 = 0$. We find that the thresholds improve for all cases when coupling is introduced for coding. Furthermore, the coupled system in coding outperforms the coupled system in BICM [34], [43], with the exception of $T_{tr} = 0$. On the other hand, the thresholds hardly improve as the coupling width W in BICM increases, as long as SC LDPC coding is used. We conclude that, for QPSK, it is sufficient to introduce coupling only in coding.

The thresholds for 16 QAM and 64 QAM are shown in Tables III and IV. We observe that coupling in BICM can provide a significant improvement in the threshold especially for 64 QAM, as well as coupling in coding. As a result, we find that the coupled system in BICM can outperform the coupled system in coding for 64 QAM, by making comparisons between the top row for $W = 2$ and the bottom row for $W = 0$ in Table IV. We shall explain why coupling should be introduced for BICM, as well as for coding. The coupled system in BICM can utilize the data symbols decoded in the preceding stages as training symbols in the current stage. The training symbols reduce inter-stream interference in MUD and allow the receiver to obtain reliable initial channel estimates. Eventually, the coupled system in BICM can attain reliable decoding results in the current stage. On the other hand, the coupled system only in coding utilizes decoding results in the preceding stages only for decoding in the current stage. For QPSK, the receiver may attain reasonably good channel estimates and detection results in the initial outer iteration. However, it may not obtain them in the initial outer iteration for higher-order modulation. As a result, the coupled system in coding has worse threshold than the coupled system in both coding and BICM or only in BICM.

We next consider how to select design parameters such as

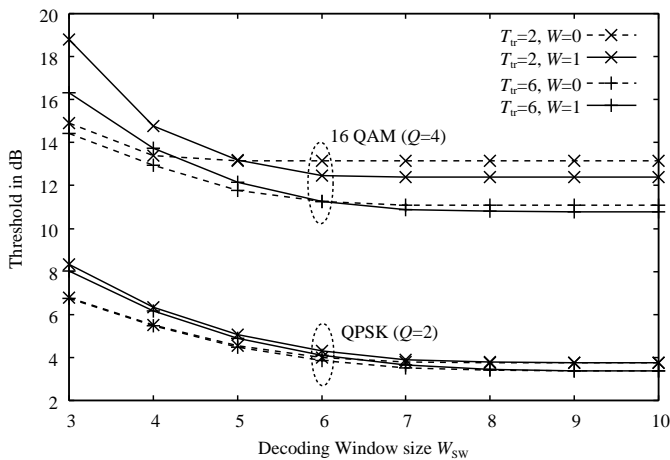


Fig. 7. Threshold versus window size W_{SW} for (3, 6, 64) SC LDPC coding, $(\infty, 64, W, Q)$ STC BICM, the SW schedule with the numbers $J = \infty$ and $I = \infty$ of inner and outer iterations, the BER requirement $\epsilon = 10^{-6}$, and 6×6 block-fading MIMO with coherence time $T = 64$.

the window size W_{SW} and the number I of outer iterations. Figure 7 shows the thresholds versus the window size W_{SW} for (3, 6, 64) SC LDPC coding. We find that the thresholds converge for $W_{SW} \geq 9$, and that the thresholds for $W = 0$ converges slightly more quickly than those for $W = 1$. Thus, an option is $W_{SW} = 9$ for achieving the ultimate threshold based on $W_{SW} = \infty$ approximately.

We investigate the minimum I_{\min} of the number of outer iterations such that the BER requirement ϵ is satisfied in all sections for an SNR $1/N_0 > \rho_{BP}$ above the threshold ρ_{BP} for infinite outer iterations $I = \infty$. In order to eliminate boundary effect, we assume infinite outer iterations for the first and last stages of the SW decoding. As shown in Fig. 8, the required number I_{\min} in the bulk region reduces quickly as the SNR $1/N_0$ increases from the ultimate threshold ρ_{BP} for $I = \infty$. We observe that the STC BICM with $W = 1$ results in smaller I_{\min} than the conventional BICM with $W = 0$. The required numbers I_{\min} for the numbers of inner iterations $J = 1$ and $J = \infty$ correspond to upper and lower bounds on the required number for a finite number of inner iterations, respectively. For example, the BER requirement is achieved by selecting the number of outer iterations $I \in [8 : 20]$ for 16 QAM and $W = 1$, when one tolerates an SNR loss of 0.35 dB from the threshold ρ_{BP} for $I = \infty$.

B. Numerical Simulations

We have so far considered the infinite code-length limit M . Next, numerical simulations for finite M are presented. For the coupled systems, we assumed the code length $M = 4QK(T - T_{tr})$ such that the frame length including pilot symbols was equal to the length of 4 fading blocks in each section. For the conventional system, on the other hand, we assumed $M = 4W_{SW}QK(T - T_{tr})$ with W_{SW} denoting the window size for the SW decoding in the coupled systems.

Figure 9 displays the average BERs in decoding versus $E_b/N_0 = 1/(RN_0)$ for QPSK. The overall rate R given by (6) is equal to $R = 5.8125$ bps/Hz for all systems.

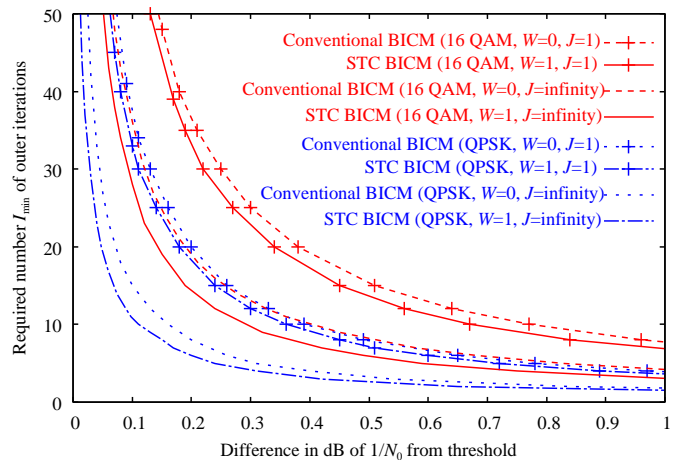


Fig. 8. Required number I_{\min} of outer iterations versus the difference $1/N_0 - \rho_{BP}$ of the SNR from the threshold ρ_{BP} for (3, 6, 64) SC LDPC coding, $(\infty, 64, W, Q)$ STC BICM, the SW schedule with the window size $W_{SW} = 9$, the BER requirement $\epsilon = 10^{-6}$, and 6×6 block-fading MIMO with coherence time $T = 64$ and the number of pilots $T_{tr} = 6$.

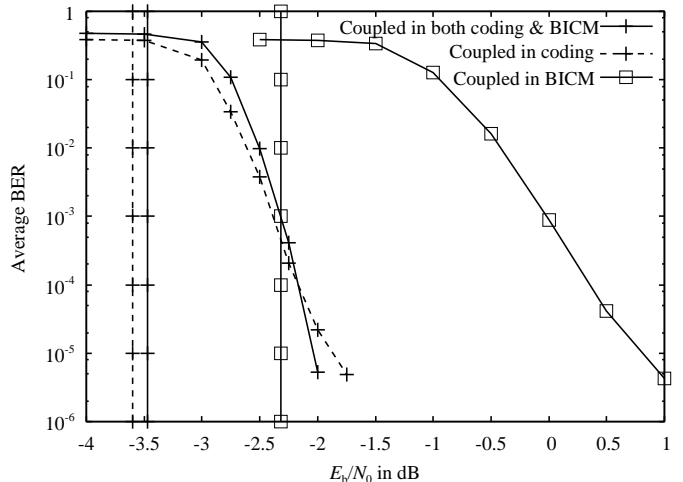


Fig. 9. Average BER versus E_b/N_0 for QPSK, the SW decoding with the window size $W_{SW} = 9$ and the numbers of inner and outer iterations $J = 4$ and $I = 20$, and 6×6 block-fading MIMO with coherence time $T = 64$. $\dot{N}_0 = N_0$ was used. (i) Coupled system in BICM: (3, 6) LDPC coding, (3024, 62, 1, 2) STC BICM, and $T_{tr} = 1$. (ii) Coupled system in coding: (3, 6, 63) SC LDPC coding, (3024, 63, 0, 2) conventional BICM, and $T_{tr} = 1$. (iii) Coupled system in both coding and BICM: (3, 6, 63) SC LDPC coding, (3072, 63, 1, 2) STC BICM, and $T_{tr} = 0$. The vertical lines represent the corresponding thresholds for the BER requirement $\epsilon = 10^{-6}$.

We omitted the conventional system that has (3, 6) LDPC coding, $(9 \times 2976, 62, 0, 2)$ conventional BICM, and $T_{tr} = 2$, since the ultimate threshold $E_b/N_0 \approx 9.7$ dB is too bad, as indicated from Table II. We find that the thresholds for the coupled systems in coding provide good predictions for the locations of the so-called waterfall regime, whereas the threshold under-estimates the location for the coupled system in BICM. One interesting observation is that the coupled system in both coding and BICM has a steeper BER slope in the waterfall regime than that only in coding. Consequently, the coupled system in both coding and BICM can achieve the best performance in the high SNR regime, even though the

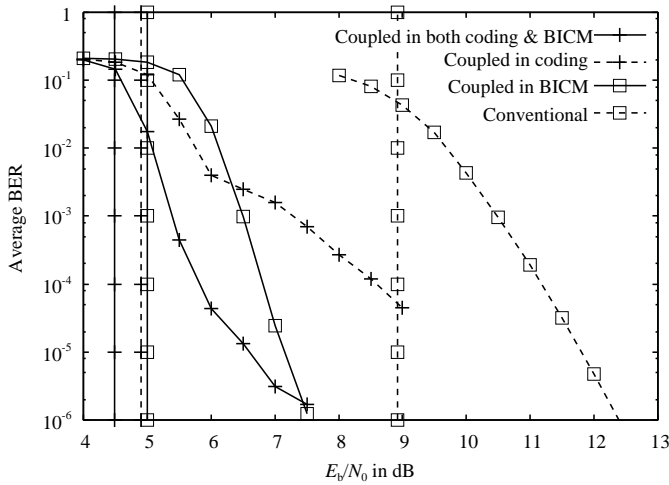


Fig. 10. Average BER versus E_b/N_0 for 64 QAM and 6×6 block-fading MIMO with coherence time $T = 64$. $1/\tilde{N}_0 = 14$ dB ($E_b/\tilde{N}_0 \approx 2.89$ dB) was used. (i) Conventional system: (3, 6) LDPC coding, ($9 \times 6624, 1, 0, 6$) conventional BICM, and $T_{tr} = 18$. (ii) Coupled system in BICM: (3, 6) LDPC coding, (6768, 46, 1, 6) STC BICM, and $T_{tr} = 17$. (iii) Coupled system in coding: (3, 6, 47) SC LDPC coding, (6768, 47, 0, 6) conventional BICM, and $T_{tr} = 17$. (iv) Coupled system in both coding and BICM: (3, 6, 47) SC LDPC coding, (6912, 47, 1, 6) STC BICM, and $T_{tr} = 16$. The coupled systems use the SW decoding with the window size $W_{SW} = 9$ and the numbers of inner and outer iterations $J = 4$ and $I = 20$, whereas $J = 12$ and $I = 60$ are used for the conventional system. The vertical lines represent the corresponding thresholds for the BER requirement $\epsilon = 10^{-6}$.

best threshold is achieved by the coupled system in coding.

Figure 10 shows numerical simulations for 64 QAM. The overall rate R is equal to $R = 12.9375$ bps/Hz for all systems. The error floor occurs remarkably for the coupled system in coding, even though the noise variance \tilde{N}_0 postulated in the channel estimator was selected so as to reduce this error floor. As a result, the two systems coupled in BICM outperform the coupled system in coding for high SNRs.

The error floor for the coupled system in coding is because the SW decoding fails to propagate in an intermediate section. In the initial outer iteration, the channel estimator has to estimate channel gains only from pilot symbols at the rightmost section of each decoding window, whereas it can utilize feedback information from the decoder in the other sections. Consequently, messages at the rightmost section are unreliable in the initial outer iteration. For finite-sized systems, the unreliable messages may propagate from right to left with a small probability. When such an unexpected propagation occurs in a stage of the SW decoding, reliable information fails to propagate from left to right.

The STC BICM can improve reliability of initial messages at the rightmost section in each decoding window, since a portion of the preceding decoding results can be utilized for the initial channel estimator at the rightmost section. This improvement results in a significant reduction of the average BER in the high SNR regime for the coupled system in both coding and BICM, as well as in an improvement of the decoding threshold.

VI. CONCLUSION

We have considered coupling in coding and BICM to improve the performance of iterative CE-MUDD. Coupling in coding results in a dominant improvement in the performance for low rate systems with QPSK. Coupling in BICM can provide additional significant gains in the waterfall and high SNR regimes for higher rate systems with higher-order modulation. We conclude that spatial coupling should be introduced for BICM in MIMO systems with higher-order modulation.

We could not conclude that spatial coupling should be introduced for *both* coding and BICM for higher-order modulation, since an error floor occurs when spatial coupling is used in coding. The analysis of this error floor is left as a future work.

APPENDIX A

EFFICIENT CALCULATION OF (17)

We shall present an efficient method for calculating (17) for all t . Let us define

$$\Xi^{\text{ch}} = \left\{ K \mathbf{I}_K + \hat{\mathbf{X}} (\Sigma^{\text{ch}} + \tilde{N}_0 \mathbf{I}_T)^{-1} \hat{\mathbf{X}}^{\text{H}} \right\}^{-1}, \quad (48)$$

with $\Sigma^{\text{ch}} = \text{diag}\{\sigma_t^2 : \text{all } t\}$, in which σ_t^2 is given by (14). Using the matrix inversion lemma³ for the identity

$$(\Xi^{\text{ch}})^{-1} = (\Xi^{\text{ch}})^{-1} - \frac{\hat{\mathbf{x}}_t \hat{\mathbf{x}}_t^{\text{H}}}{\sigma_t^2 + \tilde{N}_0}, \quad (49)$$

with $\hat{\mathbf{x}}_t$ denoting the t th column of $\hat{\mathbf{X}}$, we obtain

$$\Xi_{\setminus t}^{\text{ch}} = \Xi^{\text{ch}} - \frac{\Xi^{\text{ch}} \hat{\mathbf{x}}_t (\Xi^{\text{ch}} \hat{\mathbf{x}}_t)^{\text{H}}}{\hat{\mathbf{x}}_t^{\text{H}} \Xi^{\text{ch}} \hat{\mathbf{x}}_t - (\sigma_t^2 + \tilde{N}_0)}. \quad (50)$$

Expression (50) implies that all a posteriori covariance matrices (17) can be obtained by one calculation of the inverse matrix (48), instead of T calculations.

APPENDIX B

DERIVATION OF PROPOSITION 1

A. Formulation

The derivation of Proposition 1 is an extension of the replica method in [43]. Assume $\tilde{N}_0 = N_0$. Since the received matrix $\mathbf{Y}_{\setminus t}$ given by (13) has i.i.d. rows, without loss of generality, we focus on the first row $\vec{\mathbf{y}}_{1,\setminus t}$ and drop the subscript 1 from all variables. For notational convenience, we write the first row of the channel matrix as $K^{-1/2} \vec{\mathbf{h}}_0 \in \mathbb{C}^{1 \times K}$, with $\vec{\mathbf{h}}_0 \sim \mathcal{CN}(\mathbf{0}, \mathbf{I}_K)$. Let $\vec{\mathbf{h}}_a \in \mathbb{C}^{1 \times K}$ denote the replicas of $\vec{\mathbf{h}}_0$: $\mathcal{H} = \{\vec{\mathbf{h}}_a : a = 0, \dots, n\}$ are independent CSCG vectors with covariance \mathbf{I}_K . Let us define a function $Z_t(n, \omega)$ as

$$Z_t(n, \omega) = \mathbb{E} \left[\int e^{\omega f} \left\{ \int p(\vec{\mathbf{y}}_{\setminus t} | \vec{\mathbf{h}}_1, \hat{\mathbf{X}}_{\setminus t}) p(\vec{\mathbf{h}}_1) d\vec{\mathbf{h}}_1 \right\}^{n-2} \cdot \prod_{a=0}^2 \left\{ p(\vec{\mathbf{y}}_{\setminus t} | \vec{\mathbf{h}}_a, \hat{\mathbf{X}}_{\setminus t}) p(\vec{\mathbf{h}}_a) d\vec{\mathbf{h}}_a \right\} d\vec{\mathbf{y}}_{\setminus t} \right], \quad (51)$$

with

$$f(\vec{\mathbf{h}}_0, \vec{\mathbf{h}}_1, \vec{\mathbf{h}}_2) = \sum_{k=1}^K \{(\vec{\mathbf{h}}_0)_k - (\vec{\mathbf{h}}_1)_k\} \{(\vec{\mathbf{h}}_0)_k - (\vec{\mathbf{h}}_2)_k\}^*. \quad (52)$$

³ $(\mathbf{A} + \mathbf{BDC})^{-1} = \mathbf{A}^{-1} - \mathbf{A}^{-1} \mathbf{B} (\mathbf{D}^{-1} + \mathbf{CA}^{-1} \mathbf{B})^{-1} \mathbf{CA}^{-1}$.

In (51), the pdf $p(\vec{y}_{\setminus t} | \vec{h}_0, \hat{\mathbf{X}}_{\setminus t})$ denotes the conditional pdf for the first row $\vec{y}_{\setminus t}$ of the received matrix given by (13). Furthermore, $p(\vec{y}_{\setminus t} | \vec{h}_a, \hat{\mathbf{X}}_{\setminus t})$ for $a \geq 1$ is the conditional pdf of $\vec{y}_{\setminus t}$ after making the Gaussian approximation of the second term on the RHS of (13), given by

$$p(\vec{y}_{\setminus t} | \vec{h}_a, \hat{\mathbf{X}}_{\setminus t}) = \prod_{t' \neq t} g_{\text{CG}} \left(y_{t'}; \frac{1}{\sqrt{K}} \vec{h}_a \hat{x}_{t'}, \sigma_{t'}^2 + N_0 \right), \quad (53)$$

where $g_{\text{CG}}(\cdot; m, \sigma^2)$ denotes the proper complex Gaussian pdf with mean m and variance σ^2 . In (53), $y_{t'}$ and $\hat{x}_{t'}$ denote the $(1, t')$ -element of \mathbf{Y} and the t' th column of $\hat{\mathbf{X}}$, respectively. The variance $\sigma_{t'}^2$ is given by (14).

Lemma 1. [43, Lemma 2] *The average MSE (26) is given by*

$$\xi_{\setminus t}(l) = \lim_{n \downarrow 0} \lim_{\omega \rightarrow 0} \frac{1}{K} \frac{\partial}{\partial \omega} \ln Z_t(n, \omega). \quad (54)$$

Lemma 1 implies that evaluating the average MSE (26) reduces to calculating the quantity (54) in the large-system limit. We follow [43] to evaluate (54) with the replica method.

B. Replica Method

We first calculate (51) only for integers $n \geq 2$. The assumption of random interleaving implies that independent LLRs are fed back from the decoder for sufficiently long code length M . In other words, $x_{k,t'}$ and $\hat{x}_{k,t'}$ are independent for all k and t' in the limit $M \rightarrow \infty$. From the central limit theorem, the *individual* estimation error $K^{-1/2} \vec{h}_0(\mathbf{x}_{t'} - \hat{\mathbf{x}}_{t'})$ conditioned on \vec{h}_0 and $\hat{\mathbf{x}}_{t'}$ converges in distribution to a CSCG vector with covariance $\sigma_{t'}^2$ given by (14) in the limit $K \rightarrow \infty$. Thus, each marginal pdf $p(y_{t'} | \vec{h}_0, \hat{\mathbf{x}}_{t'})$ tends to the t' th factor on the RHS of (53) with $\vec{h}_a = \vec{h}_0$. Note that we do not claim the convergence of the joint pdf $p(\vec{y}_{\setminus t} | \vec{h}_0, \hat{\mathbf{X}}_{\setminus t})$ to (53). From these observations, we find that (51) reduces to

$$\frac{1}{K} \ln Z_t(n, \omega) = \mathbb{E} \left[e^{\omega f} \left\{ e_n(\{v_a^{\text{P}}\}, N_0, \mathcal{H}) \right\}^{T_{\text{tr}}} \cdot \prod_{t' \in (T_{\text{tr}}:T), t' \neq t} e_n(\{v_a^{\text{C}}\}, \sigma_{t'}^2 + N_0, \mathcal{H}) \right] + O(K^{-1}) \quad (55)$$

in the large-system limit, with

$$e_n(\{v_a\}, \sigma^2, \mathcal{H}) = \mathbb{E} \left[\int_{\mathcal{C}} \prod_{a=0}^n g_{\text{CG}}(y; v_a, \sigma^2) dy \middle| \mathcal{H} \right]. \quad (56)$$

In (55), v_a^{P} and v_a^{C} are respectively given by

$$v_a^{\text{P}} = \frac{1}{\sqrt{K}} \sum_{k=1}^K (\vec{h}_a)_k x_{k,1}, \quad v_a^{\text{C}} = \frac{1}{\sqrt{K}} \sum_{k=1}^K (\vec{h}_a)_k \hat{x}_{k,T}. \quad (57)$$

Recall that we are focusing on a fading block in section l . In order to evaluate the quantity $e_n(\{v_a^{\text{C}}\}, \sigma_{t'}^2 + N_0, \mathcal{H})$ in (55), we use the fact that $\sigma_{t'}^2$ given by (14) converges in probability to $\sigma_{\text{dec}}^2(l) \equiv 1 - \hat{x}_{\text{dec}}^2(l)$ given by (27) in the limit $K \rightarrow \infty$. As discussed in [43], the perturbation $\sigma_{t'}^2 - \sigma_{\text{dec}}^2(l)$ provides a negligible impact on (54) in the large-system limit. Thus, we can replace $\sigma_{t'}^2$ in (55) by $\sigma_{\text{dec}}^2(l)$ as long as the large-system limit is considered. Since the soft decisions $\{\hat{x}_{k,T}\}$ are

independent zero-mean random variables, $\mathbf{v}^{\text{C}} = (v_0^{\text{C}}, \dots, v_n^{\text{C}})^{\text{T}}$ given \mathcal{H} converges in distribution to a CSCG vector with covariance $\mathbb{E}[\hat{x}_{1,T}^2] \mathbf{Q}$, given by

$$\mathbf{Q} = \frac{1}{K} \sum_{k=1}^K \mathbf{h}_k(n) \mathbf{h}_k(n)^{\text{H}}, \quad (58)$$

where the column vector $\mathbf{h}_k(n)$ has $(\vec{h}_a)_k$ as the a th element for $a = 0, \dots, n$. It is possible to calculate the conditional expectation over \mathbf{v}^{C} after evaluating the integration in (56). Let us define the function $G(\mathbf{Q})$ as

$$G(\mathbf{Q}) = -\ln \det(\mathbf{I}_{n+1} + \mathbf{A}\mathbf{Q}) - n \ln(\pi N_0) - \ln(1+n), \quad (59)$$

with

$$\mathbf{A} = \frac{1}{1+n} \begin{pmatrix} n & -\mathbf{1}_n^{\text{T}} \\ -\mathbf{1}_n & (1+n)\mathbf{I}_n - \mathbf{1}_n \mathbf{1}_n^{\text{T}} \end{pmatrix}, \quad (60)$$

where $\mathbf{1}_n$ denotes the n -dimensional column vector whose elements are all one. Repeating the same argument for the quantity $e_n(\{v_a^{\text{P}}\}, N_0, \mathcal{H})$, we arrive at

$$\frac{1}{K} \ln Z_t(n, \omega) = \frac{1}{K} \ln \mathbb{E} \left[e^{\omega f + K \tilde{G}(\mathbf{Q})} \right] + O(K^{-1/2}), \quad (61)$$

where $\tilde{G}(\mathbf{Q})$ is given by

$$\tilde{G}(\mathbf{Q}) = \frac{T_{\text{tr}}}{K} G \left(\frac{\mathbf{Q}}{N_0} \right) + \frac{T - T_{\text{tr}} - 1}{K} G \left(\frac{\hat{x}_{\text{dec}}^2(l)}{\sigma_{\text{dec}}^2(l) + N_0} \mathbf{Q} \right). \quad (62)$$

In the derivation of (61), we have used (27).

The calculation of (61) was presented in [43] under the assumption of replica symmetry (RS). Thus, we omit the remaining calculation under the RS assumption.

REFERENCES

- [1] G. J. Foschini and M. J. Gans, "On limits of wireless communications in a fading environment when using multiple antennas," *Wireless Pers. Commun.*, vol. 6, pp. 311–335, 1998.
- [2] E. Telatar, "Capacity of multi-antenna Gaussian channels," *Euro. Trans. Telecommun.*, vol. 10, no. 6, pp. 585–595, Nov.–Dec. 1999.
- [3] C. Berrou and A. Glavieux, "Near optimum error correcting coding and decoding: Turbo-codes," *IEEE Trans. Commun.*, vol. 44, no. 10, pp. 1261–1271, Oct. 1996.
- [4] P. D. Alexander, A. J. Grant, and M. C. Reed, "Iterative detection in code-division multiple-access with error control coding," *Euro. Trans. Telecommun.*, vol. 9, no. 5, pp. 419–425, Sep.–Oct. 1998.
- [5] M. C. Reed, C. B. Schlegel, P. D. Alexander, and J. A. Asenstorfer, "Iterative multiuser detection for CDMA with FEC: near-single-user performance," *IEEE Trans. Commun.*, vol. 46, no. 12, pp. 1693–1699, Dec. 1998.
- [6] J. Pearl, *Probabilistic Reasoning in Intelligent Systems: Networks of Plausible Inference*. San Francisco, CA: Morgan Kaufmann, 1988.
- [7] J. Boutros and G. Caire, "Iterative multiuser joint decoding: Unified framework and asymptotic analysis," *IEEE Trans. Inf. Theory*, vol. 48, no. 7, pp. 1772–1793, Jul. 2002.
- [8] X. Wang and H. V. Poor, "Iterative (turbo) soft interference cancellation and decoding for coded CDMA," *IEEE Trans. Commun.*, vol. 47, no. 7, pp. 1046–1061, Jul. 1999.
- [9] P. D. Alexander and A. J. Grant, "Iterative channel and information sequence estimation in CDMA," in *Proc. IEEE 6th Int. Symp. Spread-Spectrum Tech. & Appl.*, vol. 2, New Jersey, USA, Sep. 2000, pp. 593–597.
- [10] H. E. Gamal and E. Geraniotis, "Iterative multiuser detection for coded CDMA signals in AWGN and fading channels," *IEEE J. Sel. Areas Commun.*, vol. 18, no. 1, pp. 30–41, Jan. 2000.
- [11] M. Kobayashi, J. Boutros, and G. Caire, "Successive interference cancellation with SISO decoding and EM channel estimation," *IEEE J. Sel. Areas Commun.*, vol. 19, no. 8, pp. 1450–1460, Aug. 2001.

- [12] A. Lampe, "Iterative multiuser detection with integrated channel estimation for coded DS-CDMA," *IEEE Trans. Commun.*, vol. 50, no. 8, pp. 1217–1223, Aug. 2002.
- [13] M. C. Valenti and B. D. Woerner, "Iterative channel estimation and decoding of pilot symbol assisted turbo codes over flat-fading channels," *IEEE J. Sel. Areas Commun.*, vol. 19, no. 9, pp. 1697–1705, Sep. 2001.
- [14] M. Lončar, R. R. Müller, J. Wehinger, C. F. Mecklenbräuker, and T. Abe, "Iterative channel estimation and data detection in frequency-selective fading MIMO channels," *Euro. Trans. Telecommun.*, vol. 15, pp. 459–470, 2004.
- [15] P. S. Rossi and R. R. Müller, "Joint twofold-iterative channel estimation and multiuser detection for MIMO-OFDM systems," *IEEE Trans. Wireless Commun.*, vol. 7, no. 11, pp. 4719–4729, Nov. 2008.
- [16] S. Kudekar, T. Richardson, and R. Urbanke, "Threshold saturation via spatial coupling: Why convolutional LDPC ensembles perform so well over the BEC," *IEEE Trans. Inf. Theory*, vol. 57, no. 2, pp. 803–834, Feb. 2011.
- [17] M. Lentmaier, A. Sridharan, D. J. Costello, Jr., and K. S. Zigangirov, "Iterative decoding threshold analysis for LDPC convolutional codes," *IEEE Trans. Inf. Theory*, vol. 56, no. 10, pp. 5274–5289, Oct. 2010.
- [18] S. H. Hassani, N. Macris, and R. Urbanke, "Chains of mean-field models," *J. Stat. Mech.*, no. 2, p. P02011, Feb. 2012.
- [19] K. Takeuchi, T. Tanaka, and T. Kawabata, "A phenomenological study on threshold improvement via spatial coupling," *IEICE Trans. Fundamentals*, vol. E95-A, no. 5, pp. 974–977, May 2012.
- [20] —, "Performance improvement of iterative multiuser detection for large sparsely-spread CDMA systems by spatial coupling," accepted for publication in *IEEE Trans. Inf. Theory*, 2014, [Online]. Available: <http://arxiv.org/abs/1206.5919>.
- [21] A. Yedla, Y.-Y. Jian, P. S. Nguyen, and H. D. Pfister, "A simple proof of threshold saturation for coupled scalar recursions," in *Proc. 7th Int. Symp. Turbo Codes & Iter. Inf. Process.*, Gothenburg, Sweden, Aug. 2012.
- [22] C. Schlegel and M. Burnashev, "Thresholds of spatially coupled systems via Lyapunov's method," in *Proc. 2013 IEEE Inf. Theory Workshop*, Seville, Spain, Sep. 2013.
- [23] R. El-Khatib, N. Macris, T. Richardson, and R. Urbanke, "Analysis of coupled scalar systems by displacement convexity," in *Proc. 2014 IEEE Int. Symp. Inf. Theory*, Honolulu, HI, USA, Jul. 2014, pp. 2321–2325.
- [24] K. Takeuchi, T. Tanaka, and T. Kawabata, "Improvement of BP-based CDMA multiuser detection by spatial coupling," in *Proc. 2011 IEEE Int. Symp. Inf. Theory*, Saint Petersburg, Russia, Aug. 2011, pp. 1489–1493.
- [25] K. Takeuchi, "Accelerating iterative detection for spatially coupled systems by collaborative training," *IEEE Commun. Lett.*, vol. 17, no. 3, pp. 451–454, Mar. 2013.
- [26] C. Schlegel and D. Truhachev, "Multiple access demodulation in the lifted signal graph with spatial coupling," *IEEE Trans. Inf. Theory*, vol. 59, no. 4, pp. 2459–2470, Apr. 2013.
- [27] F. Krzakala, M. Mézard, F. Sausset, Y. F. Sun, and L. Zdeborová, "Statistical-physics-based reconstruction in compressed sensing," *Phys. Rev. X*, vol. 2, pp. 021005–1–18, May 2012.
- [28] D. L. Donoho, A. Javanmard, and A. Montanari, "Information-theoretically optimal compressed sensing via spatial coupling and approximate message passing," *IEEE Trans. Inf. Theory*, vol. 59, no. 11, pp. 7434–7464, Nov. 2013.
- [29] K. Kasai and K. Sakaniwa, "Spatially-coupled MacKay-Neal codes and Hsu-Anastasopoulos codes," *IEICE Trans. Fundamentals*, vol. E94-A, no. 11, pp. 2161–2168, Nov. 2011.
- [30] A. Yedla, H. D. Pfister, and K. R. Narayanan, "Universality for the noisy Slepian-Wolf problem via spatial coupling," in *Proc. 2011 IEEE Int. Symp. Inf. Theory*, Saint Petersburg, Russia, Aug. 2011, pp. 2567–2571.
- [31] V. Aref, N. Macris, and M. Vuffray, "Approaching the rate-distortion limit by spatial coupling with belief propagation and decimation," in *Proc. 2013 IEEE Int. Symp. Inf. Theory*, Istanbul, Turkey, Jul. 2013, pp. 1177–1181.
- [32] Z. Zhang, C. Xu, and L. Ping, "Spatially coupled LDPC coding and linear precoding for MIMO systems," *IEICE Trans. Commun.*, vol. E95-B, no. 12, pp. 3663–3670, Dec. 2012.
- [33] K. Takeuchi and S. Horio, "Iterative multiuser detection and decoding with spatially coupled interleaving," *IEEE Wireless Commun. Lett.*, vol. 2, no. 6, pp. 619–622, Dec. 2013.
- [34] S. Horio, K. Takeuchi, and T. Kawabata, "Iterative channel estimation and decoding via spatial coupling," *IEICE Trans. Fundamentals*, vol. E98-A, no. 2, Feb. 2015.
- [35] T. J. Richardson and R. L. Urbanke, "The capacity of low-density parity-check codes under message-passing decoding," *IEEE Trans. Inf. Theory*, vol. 47, no. 2, pp. 599–618, Feb. 2001.
- [36] S.-Y. Chung, T. J. Richardson, and R. L. Urbanke, "Analysis of sum-product decoding of low-density parity-check codes using a Gaussian approximation," *IEEE Trans. Inf. Theory*, vol. 47, no. 2, pp. 657–670, Feb. 2001.
- [37] H. El Gamal and A. R. Hammons, Jr., "Analyzing the turbo decoder using the Gaussian approximation," *IEEE Trans. Inf. Theory*, vol. 47, no. 2, pp. 671–686, Feb. 2001.
- [38] S. ten Brink, "Convergence behavior of iteratively decoded parallel concatenated codes," *IEEE Trans. Commun.*, vol. 49, no. 10, pp. 1727–1737, Oct. 2001.
- [39] G. Caire, R. R. Müller, and T. Tanaka, "Iterative multiuser joint decoding: Optimal power allocation and low-complexity implementation," *IEEE Trans. Inf. Theory*, vol. 50, no. 9, pp. 1950–1973, Sep. 2004.
- [40] Y.-N. Lee, A. Ashikhmin, and J.-T. Chen, "Impact of soft channel construction on iterative channel estimation and data decoding for multicarrier systems," *IEEE Trans. Wireless Commun.*, vol. 7, no. 7, pp. 2762–2770, Jul. 2008.
- [41] K. Takeuchi, R. R. Müller, and M. Vehkaperä, "Iterative LMMSE channel estimation and decoding based on probabilistic bias," *IEEE Trans. Commun.*, vol. 61, no. 7, pp. 2853–2863, Jul. 2013.
- [42] M. Vehkaperä, K. Takeuchi, R. R. Müller, and T. Tanaka, "Iterative channel and data estimation: Framework and analysis via replica method," in *Proc. 2009 IEEE Int. Symp. Inf. Theory*, Seoul, Korea, Jun. 2009, pp. 2689–2693.
- [43] K. Takeuchi, R. R. Müller, M. Vehkaperä, and T. Tanaka, "On an achievable rate of large Rayleigh block-fading MIMO channels with no CSI," *IEEE Trans. Inf. Theory*, vol. 59, no. 10, pp. 6517–6541, Oct. 2013.
- [44] Mézard, G. Parisi, and M. A. Virasoro, *Spin Glass Theory and Beyond*. Singapore: World Scientific, 1987.
- [45] H. Nishimori, *Statistical Physics of Spin Glasses and Information Processing*. New York: Oxford University Press, 2001.
- [46] T. Tanaka, "A statistical-mechanics approach to large-system analysis of CDMA multiuser detectors," *IEEE Trans. Inf. Theory*, vol. 48, no. 11, pp. 2888–2910, Nov. 2002.
- [47] A. L. Moustakas, S. H. Simon, and A. M. Sengupta, "MIMO capacity through correlated channels in the presence of correlated interferers and noise: A (not so) large N analysis," *IEEE Trans. Inf. Theory*, vol. 49, no. 10, pp. 2545–2561, Oct. 2003.
- [48] R. R. Müller and W. H. Gerstacker, "On the capacity loss due to separation of detection and decoding," *IEEE Trans. Inf. Theory*, vol. 50, no. 8, pp. 1769–1778, Aug. 2004.
- [49] D. Guo and S. Verdú, "Randomly spread CDMA: Asymptotics via statistical physics," *IEEE Trans. Inf. Theory*, vol. 51, no. 6, pp. 1983–2010, Jun. 2005.
- [50] C. K. Wen and K. K. Wong, "Asymptotic analysis of spatially correlated MIMO multiple-access channels with arbitrary signaling inputs for joint and separate decoding," *IEEE Trans. Inf. Theory*, vol. 53, no. 1, pp. 252–268, Jan. 2007.
- [51] K. Takeuchi, T. Tanaka, and T. Yano, "Asymptotic analysis of general multiuser detectors in MIMO DS-CDMA channels," *IEEE J. Sel. Areas Commun.*, vol. 26, no. 3, pp. 486–496, Apr. 2008.
- [52] K. Takeuchi, M. Vehkaperä, T. Tanaka, and R. R. Müller, "Large-system analysis of joint channel and data estimation for MIMO DS-CDMA systems," *IEEE Trans. Inf. Theory*, vol. 58, no. 3, pp. 1385–1412, Mar. 2012.
- [53] T. L. Marzetta and B. M. Hochwald, "Capacity of a mobile multiple-antenna communication link in Rayleigh flat fading," *IEEE Trans. Inf. Theory*, vol. 45, no. 1, pp. 139–157, Jan. 1999.
- [54] K. Tazoe, K. Kasai, and K. Sakaniwa, "Efficient termination of spatially-coupled codes," in *Proc. 2012 IEEE Inf. Theory Workshop*, Lausanne, Switzerland, Sep. 2012, pp. 30–34.
- [55] K. Takeuchi, "A generalization of threshold saturation: Application to spatially coupled BICM-ID," in *Proc. 2014 IEEE Int. Symp. Inf. Theory*, Honolulu, HI, USA, Jul. 2014, pp. 2316–2320.
- [56] A. G. Fábregas, A. Martinez, and G. Caire, *Bit-Interleaved Coded Modulation*. Hanover, MA, USA: now Publishers Inc., 2008.
- [57] T. Richardson and R. Urbanke, *Modern Coding Theory*. New York: Cambridge University Press, 2008.
- [58] L. Schmalen and S. ten Brink, "Combining spatially coupled LDPC codes with modulation and detection," in *Proc. 9th Int. ITG Conf. Systems, Commun., & Coding*, Munich, Germany, Jan. 2013.

